Swarm LP Bias Sweeps

David Rodriguez Otero

Swedish Institute of Space Physics
Uppsala
February 2022

Master thesis (draft) at
The Royal Institute of Technology
Stockholm, Sweden

Abstract

A Langmuir probe can get its surface contaminated during its operational life, developing an external layer that significantly affects its measurements. Thus, the well-known theory of Collectors in Gaseous Discharges is no longer valid and these non-ideal conditions need to be adequately modeled. Contaminated probes show a hysteresis loop in their current-voltage characteristics that may cause a misinterpretation of the plasma parameters derived from them. This suggest the presence of an insulating external layer that brings a capacitive behaviour into the circuit. This layer is, therefore, represented by a capcitor and a leakage resistance. The primary goal of this work is to check if this model is suitable to explain the experimental measurements of the Langmuir probes carried by the three Swarm satellites and improve their plasma paramater estimates. We have found that the RC model is an adequate tool to remove the hysteresis loop found in the experimental current characteristics. The value of the capacitance of the insultaing layer is of a few microfarads, while the resistance turned out to be too high to be relevant in the measurements and it can be removed from the model. However, the RC model does not explain all the features found in the data and some of them could be explained including another surface resistance between the insulating layer and the probe. This report sets the path to the development of an improved method to derive the plasma parameters out of the Langmuir probes of Swarm mission.

Keywords

Plasma physics, measurement technology, Langmuir probe, hysteresis, surface contamination, modelling and data analysis, instrument calibration

Acknowledgements

To Anders Eriksson, who offered me this project, helped me to carry it out, with invaluable help and contributions. Also to the whole team in IRFU and specially, Thomas Nilsson.
To my whole family, specially my parents, who even in the most difficult moments have been able to support me.
Also to my friends Raquel, Daniel and Raül who accompanied and supported me in carrying out this project.

Table of Contents

Nomenclature

Abbreviations

EFI	Electric Field Instrument
ESA	European Space Agency
HM	Harmonic Mode
IRFU	Institutet för rymdfysik i Uppsala (Institute of Space Physics in Uppsala)
ISC	Incoherent Scatter Radar
LEO	Low Earth Orbit
LP	Langmuir Probe
OML	Orbital Motino Limited
SSA	South Atlantic Anomaly
TII	Thermal Ion Imager

Latin symbols

a	Probe radius
C_c	Contamination layer capacitance
E	Ion ram energy
e	Electron charge
I_{e0}	Electron thermal current
I_{i0}	Ion thermal current
I_p	Probe current
I_{pi}	Ion current
I_{pe}	Electron current
K_B	Boltzmann´s constant
m	Electron mass

m_p	Proton mass
p_1	Linear coefficient in interpolation
R_c	Contamination layer resistance
T_e	Electron temperature
t	Time
t_e	Duration of a sweep
u	First component of the velocity in a Maxwellian distribution
V_b	Bias Voltage
V_c	Contamination layer Voltage
V_F	Floating potential
V_p	Plasma Voltage
V_s	Spacecraft Voltage
v	Second component of the velocity in a Maxwellian distribution
v_d	Drift velocity
w	Third component of the velocity in a Maxwellian distribution

Greek symbols

β	Non-ideal coefficient in electron saturation region
Δt	Time step in a sweep measurement
τ	Contamination layer charge time constant

1. Introduction

The work developed during this project belongs to the area of measurement technology in space environment. It is specifically focused on data processing from Langmuir probes measurements. This data comes from in-situ measurements from Swarm satellites.

The Swarm satellites belong to the ESA mission Swarm. The purpose of this mission is to broaden humanity knowledge of the Earth´s geomagnetic field as well as to understand or explain the significant changes it4 has suffered in the last century [2]. To fulfill this goal, the satellites carry a wide variety of electric field instruments, among which is the Langmuir Probe.

Langmuir Probes can be wisely operated to derive certain parameters describing the plasma environment [3]. And, although the measurements are rather simple, their interpretation and analysis requires a deeper understanding of the Langmuir probe theory under the scientific field of the plasma physics.

However, the measurements of the Langmuir probes on Swarm satellites show irregular features that do not match with the expected results, hysteresis loops for example. This is not a new problem in this field since Langmuir Probes have already shown strong biases in their measurements when compared to other instruments [4].

This project deals with this issue, pursuing a better understanding of the measurement technique in general and looking for a improvement in the estimates of the plasma parameters from Swarm mission.

Many researchers before have found that the contamination of the surface of the probe leads to the formation of an insulating layer in the surface that greatly disturbs the measurements introducing a capacitive behaviour in the probe response [1], [5] and [6]. This layer is modeled in several previous works as an RC layer. This report will try to answer whether this model is a suitable tool to correct the data and improve the plasma parameter estimates.

The project is performed at the Swedish Institute of Space Physics, which provided the Langmuir Probes on Swarm mission to ESA. They are searching for an improved analysis method that can be implemented in the data pipeline, but all steps towards that goal are valuable, and this project stands as one of these steps.

This project does not intend to solve all the measurement problems and implement a flawless method, but to research on the measurement technique in order to get significant improvements in the derivation of the plasma parameters if the method proves successful. Essentially, this project aims to help to understand the limitations of Langmuir probes and, eventually, improve their accuracy.

2. Background

Earth´s magnetosphere plays a key role at sustaining life on Earth. The magnetic field shields the surface of the Earth from highly energetic particles that pose a threat to every living being in our planet. However, it is undergoing meaningful changes that may affect its ability to effectively protect the Earth.

Recent studies have concluded that in the last 50 years the magnetic field strength has dropped from 24000 nT to 22000 nT in the region known as the South Atlantic Anomaly, easily seen in figure 2.1. On average, over the last 200 years, the magnetic field has lost a 9 % of its strength in global terms as stated in [2]. The consequences of this weakening are already significant for satellites orbiting the Earth, whose onboard computers may suffer from the radiation they are exposed to.

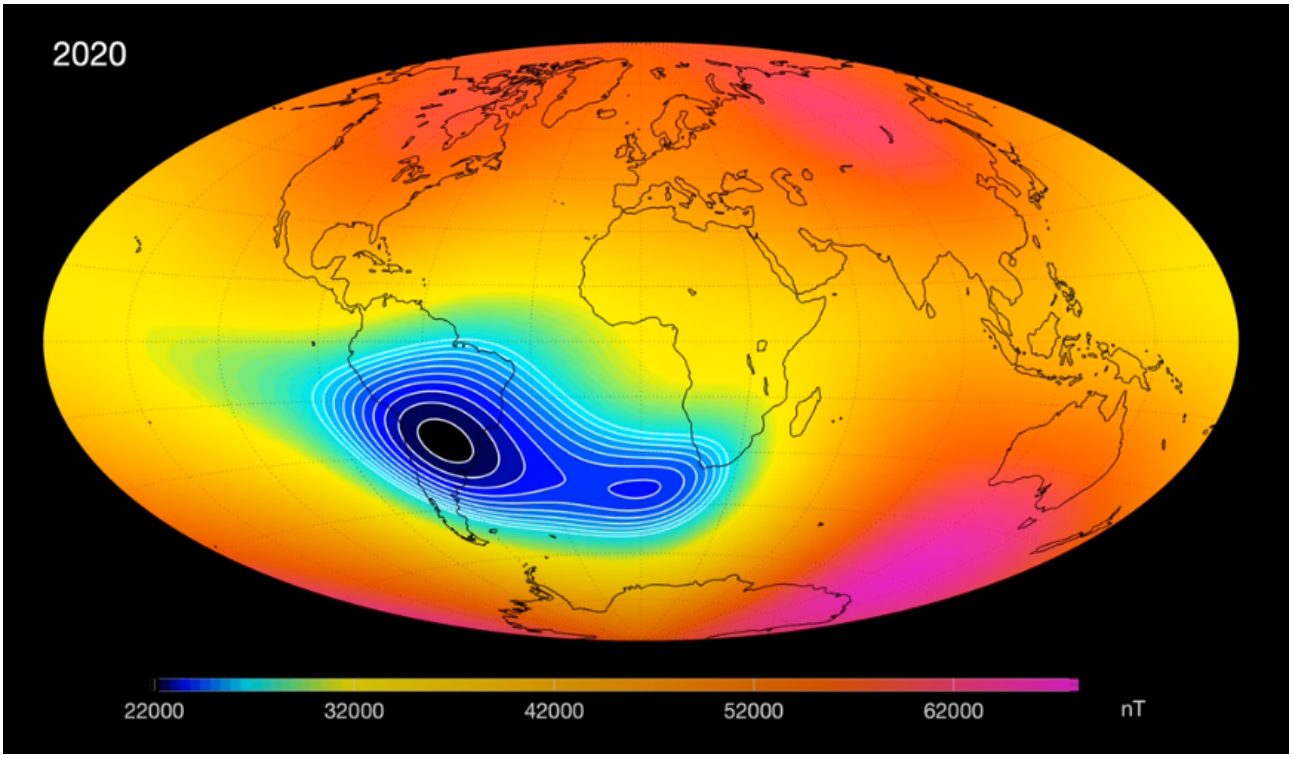

Figure 2.1: ESA,s figure showing the South Atlantic Anomaly. The magnetic field strength is displayed all over the Earth at the most recent date, year 2020. [image credit: ESA]

Understanding the nature of these changes in the magnetic field and broadening our knowledge over the Earth´s environment has driven the ESA mission Swarm.

2.1. Swarm mission

Swarm belongs to the Earth Explorer program led by ESA [7]. This program begun back in 2009 with the launching of the Gravity Field and Steady-State Ocean Explorer which was aimed at studying the gravity field. This was followed by many other missions that were dedicated to the study of different aspects of the terrestrial environment such as the water cycle, the polar caps, the magnetic field, the wind profiles, climate regulation in the atmosphere and the Earth´s biomass.

Swarm´s purpose is to further research on the Earth´s magnetic field with special interest on its weakening against solar radiation and how fast it is happening [2]. With this objective, this mission was launched on 2013 and was meant to operate for four years, though their mission was granted an extension of another four years.

Swarm mission is a constellation of three identical satellites named *Alpha*, *Bravo* and *Charlie*, hereinafter satellites A, B and C. They were placed into nearly polar, circular orbits in Low Earth Orbit. Out of the three satellites only A and C keep a similar trajectory at 460 km of altitude with a difference of $1.4^{\underline{o}}$ in latitude, whereas satellite B is in slightly higher orbit at 510 km altitude[8]. The reason behind this setting is that it is expected to maximize the scientific outcome of the mission. This configuration is artistically shown in figure 2.2.

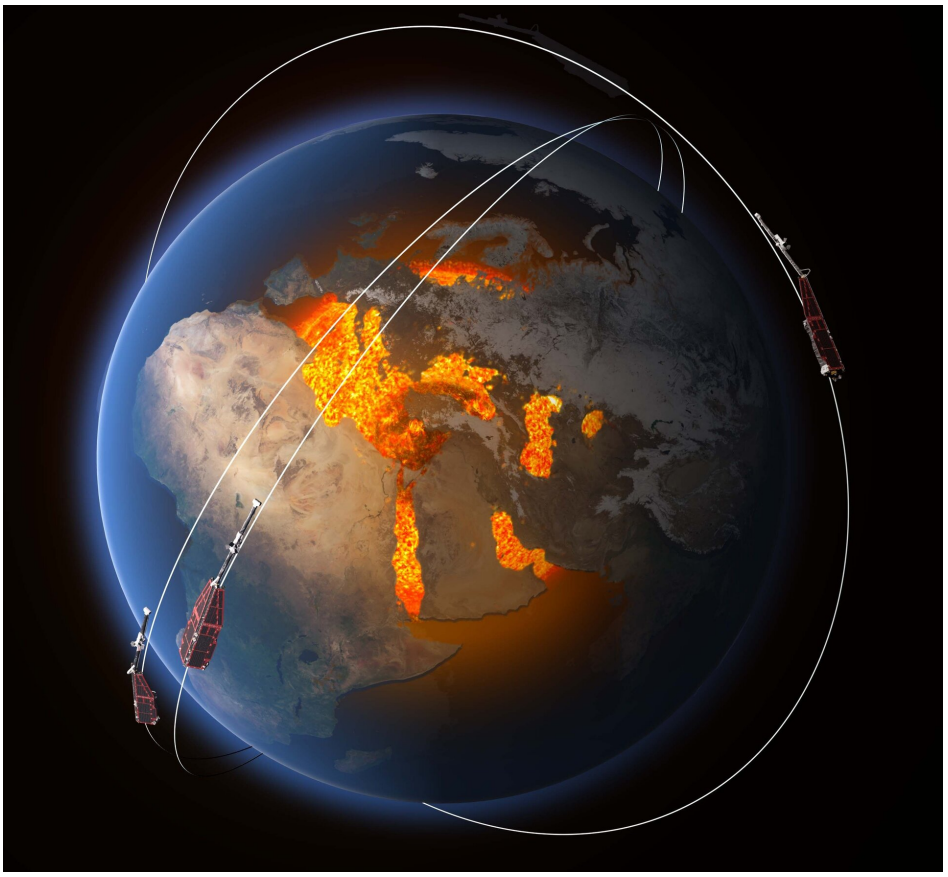

Figure 2.2: ESA´s figure representing the configuration of the orbits of the three Swarm Satellites. [image credit: ESA]

Each of the Swarm satellites carry an Electric Field Instrument located in the leading side of the satellite and aimed at describing the electrical field around the Earth. It carries two different components: the Langmuir Probe and the Thermal Ion Imager. The latter provides information about the ion drift velocity, while the Langmuir Probe allows to determine plasma parameters such as density and temperature as well as the spacecraft potential.

Langmuir Probe on Swarm satellites

Swarm satellites carry two Langmuir Probes that are located at the front on the nadir face of the spacecraft. The two of them are mounted on the spacecraft keeping a significant separation between them. This configuration is shown in figure 2.3.

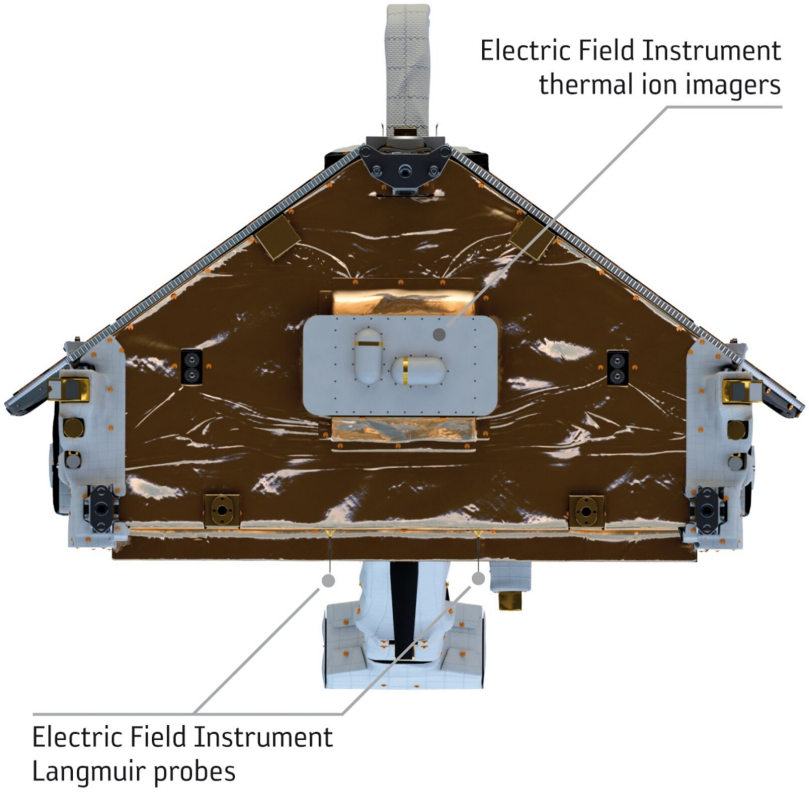

Figure 2.3: ESA´s figure of a Swarm satellite describing the position of the EFI components: the TII and the LP. [image credit: ESA]

Swarm Langmuir Probes are spherical and solid, with a radius of 4 mm. These spheres are mounted on short rods that are adequately fixed to the spacecraft body. The surface materials of these spheres is also different: while one is made of nitrated titanium (TiN), the other sphere went through a electroplating process with gold (Au). Initially both probes were meant to have a TiN sphere, but reports of possible issues with atomic oxygen for this material motivated the exchange of one of the probes in each spacecraft.

Langmuir Probes on Swarm satellites have two different operation modes, the classical sweep analysis and the Harmonic Mode.

In the sweep mode, the goal is to obtain the so-called I-V curve that allows to derive the main properties of the plasma. This curve describes how the collected current in the probe varies according to the potential difference applied between the probe and the spacecraft gorund. Thus, in this mode, a time-varying potential is applied to the probe, recording in each step the value of the current measured. The range of the sweep has been mostly set to $\pm 5V$ or from $-1{,}5V$ to $2{,}5V$. Only in the latter case, the sweep is performed twice, first with increasing voltage and then with decreasing voltage. These sweeps are done every 128 seconds and only last 1 second, no matter which of the described ranges is being used.

The other operation mode is the Harmonic Mode. This employs most of the operating time, 127 seconds every 128. The objective of this new mode is to get the measures of the current in three specified points: the first one at very low potential bias so that only the ion current is relevant, the second one at the linear electron region, where the electron current is saturated at large positive potentials and the last one in the retarded electron region, below the knee on the current characteristic. The harmonic modulation allows to get the current and the admittance in each point that contains information about the derivative of the I-V curve.

The equations of the Langmuir Probe current collection theory can be arranged properly and eventually solved to obtain the values of the plasma parameters with the three set of values (voltage, current and the derivative) measured. The temperature and densities estimates derived from this method have shown a bias with respect to other measurements [8] similar to that found with the sweep operation mode (This will be further discussed).

In addition, the Harmonic Mode is capable of measuring the capacitance of the system and thus it represent a tool to estimate different disturbances present in the probe environment.In this repot, we will only use the sweep mode, as it provides the most complete information about the probe performance.

2.2. Theory of Langmuir Probes current collection

Langmuir probes operating in the sweep analysis have, as previously discussed, the main objective to record the I-V characteristic curve. Then, using suitable expressions it can lead to relevant plasma parameters. The Langmuir probe current collection theory is a well established theory introduced in 1926 by Mott Smith and Langmuir [3]. It is however incomplete since the parameters defining the behaviour of the plasma strongly vary among the different situations one may encounter in plasma environments [9]. It is required to set the assumptions and the limits where the analysis is being done and the scope and validity of the expressions being used.

Swarm satellites are located in LEO, travelling through the Earth´s ionosphere. This a cold plasma environment with temperatures below 1eV. This implies that the thermal motion of the ions is much slower than the spacecraft speed (about 7 km/s) and therefore can be neglected in the formulation of the problem. Besides the electrical charge density in the ionosphere is zero.

At distances greater than the Debye´s (at most a few centimeters in Swarm orbit) length the ion number density and the electron density are approximately equal ($n_e \simeq n_i = n$). In short, the environment of the probes is a cold and quasi-neutral plasma.

When the probe is negatively biased with respect to the plasma medium it collects mainly ions, and when, on the contrary, it is positively charged it attract electrons. Then, the total current through the probe is divided into two different sources:

$$I_p(V_p) = I_{pi}(V_p) + I_{pe}(V_p) \tag{2.1}$$

The expressions for these were first derived in 1926 by Mott Smith and Langmuir using the Orbital Motion Limited theory (OML). This theory assumes the '*electrode*', which is the probe, to be immersed in a collisionless plasma. Then the currents can be derived from the velocity distribution of the species in the plasma.

Assuming the electrons velocity answers to a Maxwellian distribution,

$$f(u,v,w) = n\left(\frac{m}{2\pi e T_e}^{\frac{3}{2}}\right) e^{-\frac{m}{2eT_e}\left(u^2+v^2+w^2\right)} \tag{2.2}$$

their motion is completely determined through its temperature.

The velocity distribution can be integrated to derive the flux of electrons through the probe. Then, the current in the probe is easily obtained including the size of the probe (the surface). This integration can be found in [10] or [3]. Eventually, the electron random current due to the electron thermal motion to an *uncharged* probe is given by

$$I_{e0} = 4\pi a^2 n e \sqrt{\frac{eT_e}{2\pi m_e}} \tag{2.3}$$

The variable T_e is the electron temperature and it must be used in units of electronvolts [eV]. The conversion from electronvolts to Kelvin is trivial:

$$T_e[eV] = \frac{K_B}{e} T_e[K] \tag{2.4}$$

where K_B is the Boltzmann constant.

The geometry of the probe is also relevant in expression 2.3 that shows the current to be proportional to the surface area of the probe ($4\pi a^2$), where a is the radius of the probe.

When it comes to calculate the current to a charged probe, it can be as well derived from the integration of the distribution function. This integration is detailed in previous studies

and specifically in reference [10]. The following equations shown here are slightly modified expressions of those resulting of the integration in [10]. They are similar to those used in more recent studies [11].

$$I_e = \begin{cases} I_{e0} e^{\frac{V_p}{T_e}} & \text{if} \quad (V_p < 0) \\ I_{e0}\left(1 + \frac{V_p}{T_e}\right) & \text{if} \quad (V_p > 0) \end{cases} \tag{2.5}$$

In this expression, the potential of the probe is included in the variable V_p which is the potential of the surface of the probe with respect to the surrounding plasma. If this potential is set to zero, what should be left is the random current due to thermal motion obtained in 2.3.

Regarding the ion current, it has been assumed that its thermal motion is to be neglected. However, it is not zero because the satellite is travelling at high speed through the plasma. This flowing plasma causes the probe to collect an ion current. This phenomenon is described in detail in reference [10] and [3]. The ion current is then given by:

$$I_i = \begin{cases} -\pi a^2 e n v_d (1 - 2\frac{eV_p}{mv_d^2}) & \text{if} \quad (V_p < \frac{mv_d^2}{2e}) \\ 0 & \text{if} \quad (V_p > \frac{mv_d^2}{2e}) \end{cases} \tag{2.6}$$

This equation introduces a new variable which describes the flowing plasma: the drift velocity, v_d. This is the absolute value of the speed of the particles in the environment. In the case of Swarm satellites this would be determined by the orbital speed of the satellites around the Earth, that is known and constant.

Equation 2.9 shows a structure similar to the electron current for positive potentials, equation 2.5. What in equation 2.5 is the thermal energy is replaced in equation 2.9 for the ram energy, E,

$$E = \frac{m}{2e} v_d^2 \tag{2.7}$$

and the random current being defined now as

$$I_{i0} = \pi a^2 e n v_d \tag{2.8}$$

Thus, the final expression, which is goins to be used in this report is:

$$I_i = \begin{cases} -I_{i0}(1 - \frac{V_p}{E}) & \text{if} \quad (V_p < E) \\ 0 & \text{if} \quad (V_p > E) \end{cases} \tag{2.9}$$

2.3. Initial data analysis

Swarm has been operating since December 2013. At this point in time, the information stored, from the Langmuir Probes alone, has grown to approximately 440GB in size. This includes the results of the measurements of both operation modes, although the vast majority correspond to the Harmonic Mode data. It does not seem efficient to work against this file both in terms of time and also space, specially considering that the purpose of the project is to analyse only the sweep measurements.

In order to solve that issue, researchers at IRFU (special mention to Thomas Nilsson) had previously created a sufficient number of files containing only information about the sweeps. These files are much smaller, more manageable and more useful since they lack superfluous information and the data is already converted and given in SI units. Besides, some issues such as overflows in the probes are identified and removed from the data, leaving cleaner measurements samples.

Each file containsdata from one day. Since the sweeps are done once every 128 seconds, it is expected to obtain around 675 arrays of data in each file. The file names unequivocally identify which satellite took the measurement and the time of that measurement, as it is shown in the following random example:

$$SW\_EXTD\_EFI\mathbf{A}\_LPSIV\_\mathbf{20180810}T000054\_20180810T235846\_0101.cdf$$

This measurement belongs to satellite A and took place on August 10 as shown in the text in bold.

Among other information such as the gain in each of the instruments, the files provide the arrays of voltage and current in both probes separately. By way of illustration, it is shown the curve obtained in a selected measurement of that file in figure 2.4. This selection is done in order to avoid irregularities later on discussed in this report.

Figure 2.4 represents a real example of the I-V curves theoretically given by the Langmuir current collection theory already described. In the figure, as the reader may have noticed, the curve is clearly divided in different regions according to the behaviour of the current.

The first region corresponds to low voltages, where the current consists mainly of ions and shows a linear behaviour. This region is the **Ion Saturation Region**. Similarly, for high voltages the current consists essentially of electrons and the I-V curve behaves linearly too. This is the **Electron Saturation Region**. In between it is found the **Electron Retardation Region** that develops from a voltage equal to the plasma potential towards lower voltages. In this region the electron motion is retarded by the negative charge in the probe surface.

This qualitative description of the graph is essential for the processing of Langmuir Probe´s measurements since it allows to split the data and derive the plasma parameters in a simple and feasible way.

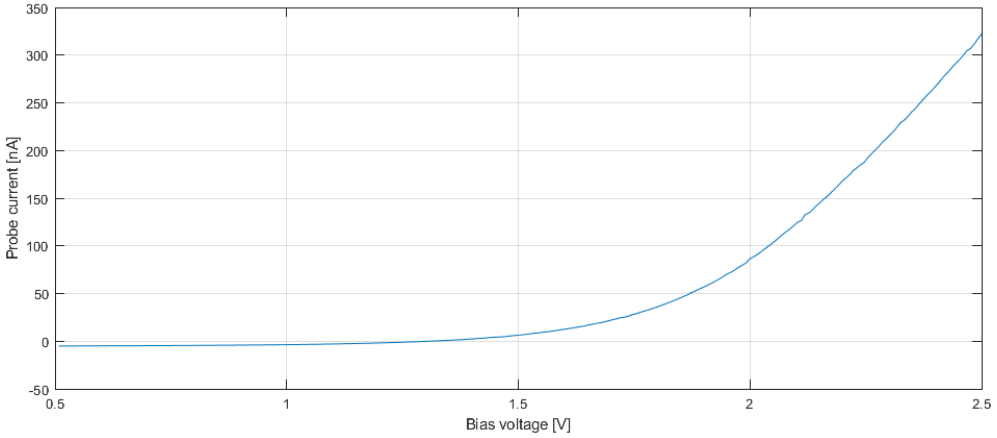

Figure 2.4: Current characteristic of probe 1 with a single sweep from 0.5V to 2.5V. Data from satellite A on 29-Oct-2018 at t = 7h17′43″.

Brief comparison theoretical I-V curves with the experimental data

The Langmuir current collection theory allows to determine the I-V curves based on several parameters including the state of the plasma or the shape and size of the probe. Thus, two geometrically identical probes working in the same environment, meaning that the plasma parameters are invariant between the two probes´environment, should ideally provide identical I-V curves as a result of the measurement.

Each of the three satellites carry two probes allowing to compare the results of simultaneous measurements of both probes and check if they provide consistent current characteristics. A quick review of the data reveals that this is not the case in Swarm satellites. Figure 2.5 shows a case of this issue. The first impression one may take for the graph is that the disagreement is larger for greater currents while being unnoticeable for very small ones.

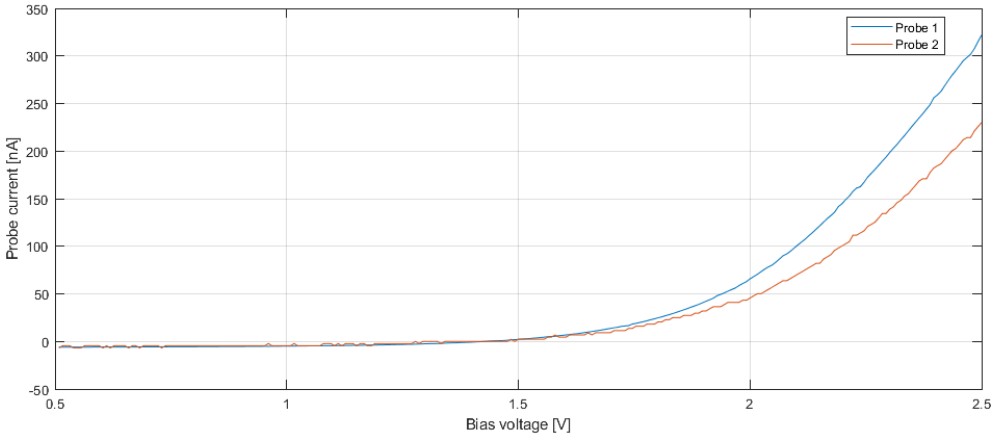

Figure 2.5: Comparison of current characteristics of both probes in simultaneous measurements. The measurement was made with a single sweep from 0.5 to 2.5V. Data from satellite A on 29-Oct-2018 at t = 8h57′59″.

The most obvious consequence of this feature is that when the usual schemes to derive the plasma parameters are applied to each of these curves, different values are to be obtained from each probe measurement. This suggests the presence of a disturbance that is not taken into account properly.

It has been said that the current measured in the probe in the simplest formulation is a function of few variables. For a given moment, when a particular voltage is applied, the value of the current drained in the probe is unique regardless of previous states of the instrument. In other words, the current state of the probe does not depend on the path the voltage followed to reach it, but only on the instantaneous voltage itself.

In the second set of sweeps (those with increasing and decreasing voltages, see LP operation) it has been observed that the value of the current for a given voltage was not the same when measured in the increasing-voltage section of the sweep than in the decreasing-voltage one. In particular the first section, with increasing voltage, provides a higher current. Figure 2.6 is shown as an example of this behaviour.

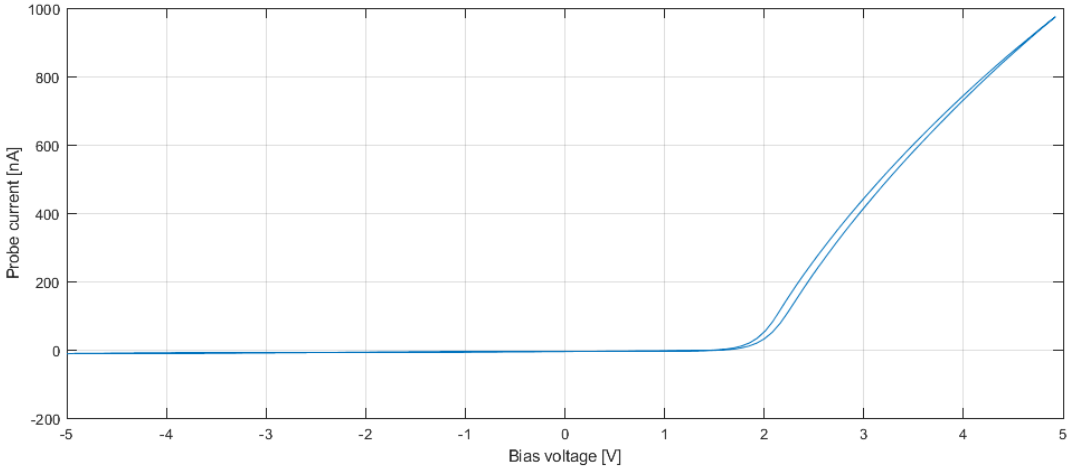

Figure 2.6: Current characteristic of probe 1 with a double sweep, forward and backward, showing the hysteresis loop. Data from satellite A on 29-Oct-2018 at t = 17h15′03″.

The curve in figure 2.6 clearly shows this behaviour. The result is a loop that resembles an hysteresis loop, which arises precisely when a function depends on its own history. This feature is of great interest since it indicates the presence of a capacitive component in the measurement system. Furthermore, this behaviour is consistent with previous studies that have shown the relationship between the hysteresis loop and the presence of surface contamination.

According to [1]: '*Variations in the probe´s surface condition can manifest themselves by hysteresis in the I-V characteristic*', which can be seen in figure 2.7. It is also mentioned that it happens when a '*symmetric sawtooth*' bias voltage sweep is applied, which is the case for Swarm. Finally, in this report, this behaviour is said to be associated to a surface contamination layer through the '*layering of foreign material on the surface of the probe*'.

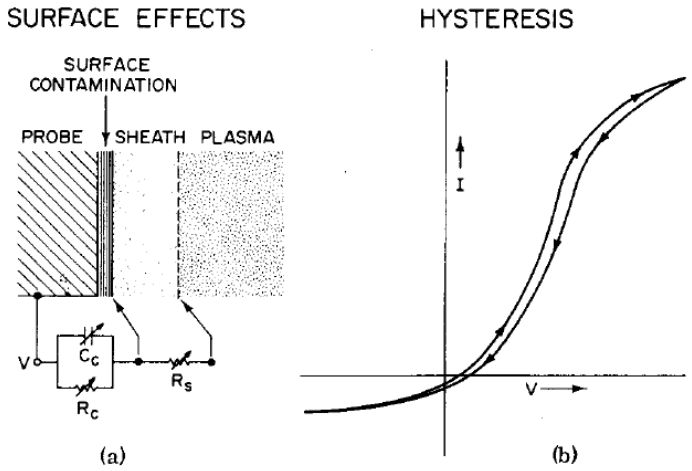

Figure 2.7: (a) Effective circuit equivalents in phenomenological model for surface contamination. (b) Hysteresis effects in conventional Langmuir probe current-voltage characteristic resulting from layering of surface contaminants. Figure from reference [1]

In [5] the authors also dealt with the issue of surface contamination on Langmuir Probes. It is said that, although the composition of the surface layer may not be known, some assumptions are made in order to conclude that the layer acquires a *large dielectric constant*, and, thus, the capacitive behaviour.

As a result of this analysis, the usual expressions for the current collected in the probe are no longer valid. The theory assumes that there is no chemical interaction between the environment and the surface of the probe [9]. This hypothesis is clearly broken due to the contamination of the probe surface that develops a dielectric layer which, in turn, causes the capacitive behaviour in the current characteristics.

Therefore, the theory needs to be modified in order to include that behaviour in the analytical expressions. The modelization of the dielectric layer is of the utmost importance to achieve more accurate estimates of the plasma parameters. The usual approach ,[1] and [5] is to modify the equivalent electric circuit of the Langmuir Probe, including an RC component between the probe and the plasma environment. This RC component consist of a capacitor, C_C associated in parallel with a leakage resistance, R_C. This circuit is schematically drawn in figure 2.7.

This approach has been also used in a precious student project on the Langmuir Probe carried on Rosetta, where the surface contamination layer disturbed the measurements [12]. Thus, this will be the approach that is going to be tested in this report in order to check whether it is consistent with the irregularities found in the data and if it can be used to improve the accuracy of the estimates derived from them.

Besides, Langmuir Probes have been found to show a tendency to overestimate electron temperatures. According to [4], it is still found in '*relatively recent measurements*'. That report precisely focuses on Swarm Langmuir Probes. The authors compared the LP estimates with the plasma parameters obtained by Incoherent Scatter Radar and found the electron temperature

to be inconsistent. Depending on the exact operational mode the T_e values were 700-900K or 300-400K higher.

The origin of this bias in Langmuir Probes might, at least partly, be found in the surface contamination layer. According to [1], this layer disturbs the estimates derived from the Langmuir Probe measurements in such a way that the electron temperature turns out to be higher than the actual one: '*conventional Langmuir Probes have indicated 'hotter' electron distributions than actually present in the ambient medium and hotter distributions than those measured by a 'clean' probe*'.

Be that as it may, what can be derived from this initial analysis is that the contamination layer greatly disturbs the operation of the Langmuir Probes, causing at least some of the problems that arise when processing their measurements. That demands for a better understanding of the effects of this layer as well as an appropriate modelling in order to derive more accurate estimates from the probes.

3. Method

The usual equations provided for the Langmuir Probe current collection previously described have been shown to be unsuitable to correctly predict the behaviour of the currents through the probe in the presence of a contamination layer. As pointed out in the references [1] or [5], this can be addressed including a capacitor and a resistance in the electrical circuit of the instrument.

The first step is, therefore, to derive the modified expressions that provide the current as function of the bias voltage applied to the surface of the probe. In these equations, the resistance and the capacitance will stand as two unknown parameters. These equations are derived from equivalent electric circuit of the probe, which is, in first place, described.

Then, the equations modelling the behaviour of the probe when it is covered by a contamination layer will be simulated and compared to the curves of a *'clean probe'*, when either there is no contamination on the surface of the probe or it has been properly removed. The behaviour of the model is then compared to the experimental curves.

Once it is confirmed the model to be suitable to fit the features on the experimental data, it can be properly used to derive the parameters that characterize the surface contamination layer: the capacitance and the resistance. This is done through an optimization method further described below using the Matlab Optimization Tool.

Finally, if the method proves successful, the hysteresis loop should be removed and then the I-V curve is ready to be fitted to the theoretical expressions in order to derive the value of the plasma parameters. There are standard procedures for this fitting process that have evolved through different missions. The methods used will be described in detail and new approaches are going to be presented in this report.

The procedure eventually described in this section will be ready to be applied in several measurements, in different satellites and years and thus, it would be possible to discuss whether the model is suitable and if the estimates improved with respect to the previous method.

3.1. Electric circuit

In a clean probe, the probe voltage with respect to the plasma, hereinafter called V_p, is directly determined through the spacecraft voltage, V_s, and the bias potential generated in the instrument, V_b. The contamination of the surface generates an insulating layer that introduces a capacitor, and a leakage current, between the probe bias voltage and the plasma sheath.

The equivalent electrical circuit of the instrument is shown in figure 3.1. The spacecraft potential is represented as a battery. This means that it is considered constant, that is does not

vary with time. In fact, it may vary over large time scales, for example over one orbit, in the order of some hours. What this assumption demands is the spacecraft voltage to be constant for the duration of the measurement: one second. In principle, it seems a reasonable assumption to simplify the analysis.

The bias voltage is represented by a variable voltage source and its variation in time is known and commanded by the instrument. The plasma sheath is shown here as a current generator. There is no clear agreement on how to treat the sheath around the probe, previous studies have modelled it as a diode, [5], or as a variable resistor, [1]. Nevertheless, the current is clearly defined by the equations of the LP current collection theory and they can be easily included in the equations regardless of how they are represented in the circuit.

Finally, the surface contamination layer is included between the probe and the plasma sheath. It consists of a capacitor of capacitance C_c and a resistor of resistance R_c placed in parallel in the circuit. The capacitor represents the insulating layer and the resistance account for the leakage current of this layer.

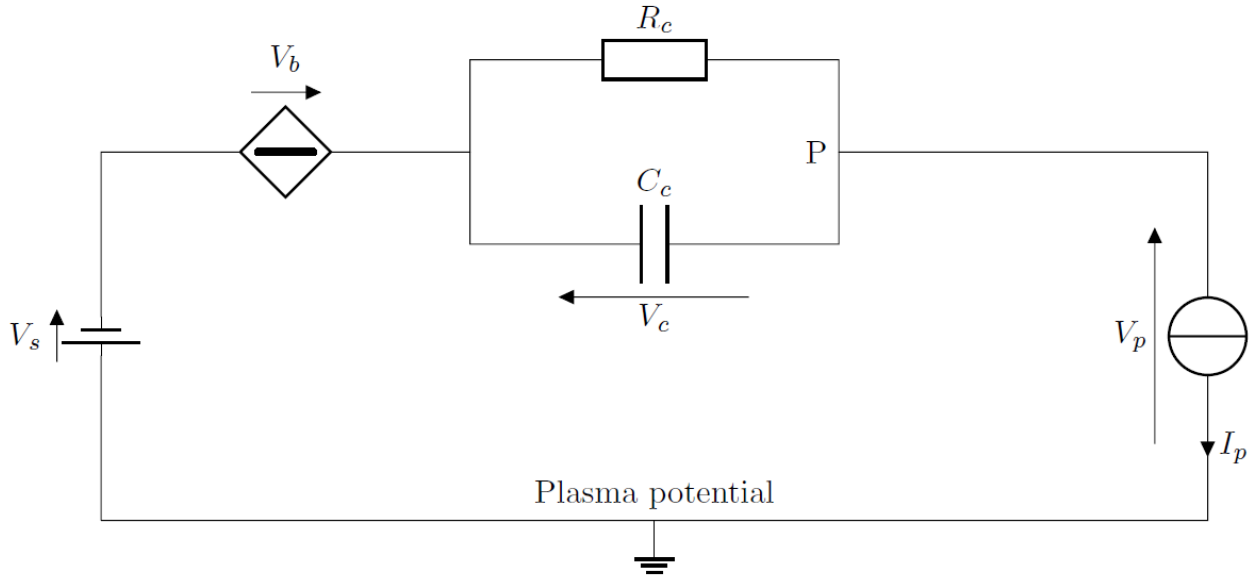

Figure 3.1: Equivalent electrical circuit of the Langmuir Probe environment including the surface contamination layer modelling.

The first obvious equation derived from the circuit is the voltage balance, or Kirchhoff´s second law, that leads to the following expression:

$$V_s + V_b = V_p + V_c \tag{3.1}$$

The second relevant equation is obtained applying the Kirchhoff´s first law, known as Kirchhoff´s nodal rule, in node P. The expressions for the current through a resistor and a capacitor are used with no further explanation.

$$\frac{V_c}{R_c} + C_c \frac{dV_c}{dt} - I_p = 0 \tag{3.2}$$

One of the assumptions made with this formulation is that both the capacitance and the resistance are constant. This, as explained with the spacecraft voltage, means that although they may change in greater scale times, they remain invariant for the duration of the measurement. The next step is to include the information of the plasma current and rearrange properly to obtain:

$$C_c\frac{dV_c}{dt} = -\frac{V_c}{R_c} + \begin{cases} I_{e0}e^{\frac{V_s+V_b-V_c}{T_e}} - I_{i0}(1-\frac{V_s+V_b-V_c}{E}) & if \quad (V_s+V_b-V_c<0) \\ I_{e0}\left(1+\frac{V_s+V_b-V_c}{T_e}\right) + I_{i0}(1-\frac{V_s+V_b-V_c}{E}) & if \quad (0<V_s+V_b-V_c<E) \\ I_{e0}\left(1+\frac{V_s+V_b-V_c}{T_e}\right) & if \quad (V_s+V_b-V_c>E) \end{cases} \tag{3.3}$$

Expression 3.3 is a non linear differential equation that has no complete solution (Regarding the last interval one may notice it is linear and it is possible through some algebra reach an analytical expression for this section of the curve). Besides it is important to highlight that it also includes a time varying term whose expression changes after reaching the maximum bias voltage, increasing the complexity of the equation.

However, considering just the electron saturation region of the curve equation 3.3 is reduced to:

$$C_c\frac{dV_c}{dt} = -\frac{V_c}{R_c} + I_{e0}\left(1+\frac{V_s+V_b-V_c}{T_e}\right) \tag{3.4}$$

And getting rid of the forcing function in this expression, one gets the homogeneous differential equation:

$$\frac{dV_c}{dt} + \left(\frac{1}{R_cC_c} + \frac{I_{e0}}{C_cT_e}\right)V_c = 0 \tag{3.5}$$

This equation gives the time constant of the system which is:

$$\tau = \left(\frac{1}{R_cC_c} + \frac{I_{e0}}{C_cT_e}\right)^{-1} \tag{3.6}$$

What stands out first is the presence of the term $\frac{1}{R_cC_c}$ that is the usual time constant when dealing with capacitors. A first estimate of the value of this constant using typical values found in [5] for the resistance and the capacitance yields:

$$\tau \simeq 1\mu F \cdot 10k\Omega = 10ms \tag{3.7}$$

This is therefore the typical time for the layer to charge and discharge itself, and therefore, to show its effects on the measurements. As previously said, each sweep measure 256 steps in one second, giving a time per step of 4ms, which is, as expected in the order of magnitude as the time constant of the capacitor charge process.

3.2. Numerical simulation

It seems obvious that the best approach to solve equation 3.3 is through numerical integration. The purpose of this is to understand how the new variables, C_c and R_c modify the current characteristic of the 'clean' probe, which is the extent of their impact and whether or not it may match the behaviour observed in the experimental data.

Numerical integration schemes, such as Euler in the simplest case, require differential equations to be in the form of:

$$\frac{dy}{dt} = f(y,t) \tag{3.8}$$

The first step to achieve this is to rearrange equation 3.2:

$$\frac{dV_c}{dt} = \frac{I_p(V_c, V_b(t))}{C_c} - \frac{V_c}{R_c C_c} \tag{3.9}$$

Equation 3.9 shows a great resemblance with equation 3.8. The right side of the equation just depends on time and the function itself. However, it becomes necessary to properly define the bias voltage function. It has been said that the hysteresis has been observed in the double sweep, which starts at -5V, increasing up to 5V and returning back to the initial point in -5V. Mathematically, this is represented by the following expression:

$$V_b = \begin{cases} -5 + 20\frac{t}{t_e} & if \quad \left(0 < t < \frac{t_e}{2}\right) \\ 15 - 20\frac{t}{t_e} & if \quad \left(\left(\frac{t_e}{2}\right) < t < t_e\right) \end{cases} \tag{3.10}$$

This equation describes the bias voltage applied in the probe as a function of time. The expression uses the variable t_e that is defined as the duration of the sweep. The sweep starts at $t = 0$ with a negative voltage of -5V. The voltage keeps increasing until it reaches a maximum at $t = t_e/2$ seconds of 5V. Then it returns to the initial point at the end of the sweep in $t = t_e$. This time, as previously said and according to literature [8], is of 1 second. This 'triangular' or 'sawtooth shaped' function is shown in figure 3.2

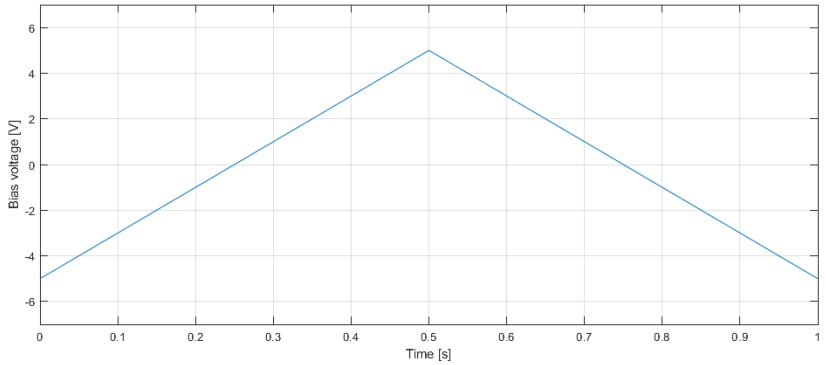

Figure 3.2: 'Triangular' or 'sawtooth shaped' function of bias voltage applied in the probe.

This can be applied in equation 3.9 to get a simulation of the current characteristic of a contaminated probe using this model. Before, one must set the environment and this includes both assuming typical values for the plasma parameters as well as defining the geometry of the probe. These are listed in table 3.1.

Physical constants	Elementary charge [C]	Electron mass [Kg]	Proton mass [Kg]
	$1{,}6022 \cdot 10^{-19}$	$9{,}1094 \cdot 10^{-31}$	$1{,}6726 \cdot 10^{-27}$
Plasma parameters	Electron Temperature [eV]	Plasma density $[cm^{-3}]$	
	0.17	10^{10}	
Satellite and instrument	Orbital speed [km/s]	Spacecraft Voltage [V]	Probe radius [m]
	7.65	0	0.004

Table 3.1: Values for the different variables of the problem: a) Physical constants, b) plasma parameters and c) Satellite and instrument.

The first row of the table just mentions the values of common and well-known physical constants. The second row of the table includes typical values expected to be found in the Swarm environment. The values come from Incoherent Scatter Radar (ISC) measures from the ground [4] that were used to validate Swarm data. The values extracted from the report were $10^4 cm^{-3}$ and $2000K$ (converted to eV according to 2.4).

Regarding the satellite and the probe characteristics only three values are required with this formulation. Satellites A and C are placed in a lower orbit and travel at 7,65km/h while satellite B is in a higher orbit with a slightly lower speed of 7,61km/h. For a qualitative analysis this minor difference is irrelevant. The second value related to the satellite is the voltage. It was set to zero since its only effect is to shift the curve horizontally and has no meaningful impact on simulation. Lastly, the probe itself only enters in the equations through the radius of the sphere at its tip.

Although it seems that everything is settled to run the simulation, there is one aspect that requires further analysis. When it comes to calculate the ion ram energy, according to equation 2.7, it is necessary to determine the ion mass, which implies, in the end, to know the composition of the environment of the probe. The satellite is orbiting the Earth at around 500km of altitude. At this height the ionosphere is composed mainly of O^+ and also, to a lesser extent, of He^+ and H^+, as shown in [13]. For simplicity, only one species, the dominating one, O^+, is considered in this analysis. Atomic oxygen has an atomic mass of 16u, yielding an ion ram energy of:

$$E = \frac{16 \cdot 1{,}6726 \cdot 10^{-27}}{2 \cdot 1{,}6022 \cdot 10^{-19}} 7650^2 \simeq 4{,}89eV \tag{3.11}$$

Finally, all the parameters of equation 3.9 are defined and it can be integrated in order to assess the impact of the values of the resistance and capacitance of the contamination layer. Besides, it will allow us to qualitatively validate the model with the experimental data. This will be done in section 4.1.

3.3. Processing of experimental data

The experimental data from Langmuir probes provide, according to the circuit in figure 3.1 the bias voltage, V_b and the probe current, I_p, both as functions of time. Equation 3.2 is a differential equation which yields the voltage across the contamination layer as a function of the probe current. Thus, it should be possible to compute this voltage drop in the surface layer with the data available in the sweeps.

There are plenty of ways to address this issue and achieve a functional numerical scheme to obtain a valid solution to differential equation 3.2. Here is presented only one of the possibilities, which tries to simplify the integration. The first step is to solve the equation for the probe current:

$$I_p = C_c \frac{dV_c}{dt} + \frac{V_c}{R_c} \tag{3.12}$$

The right hand of the equation can be wisely simplified using the following equality:

$$\frac{d(V_c e^{\frac{t}{R_c C_c}})}{dt} = e^{\frac{t}{R_c C_c}} \frac{dV_c}{dt} + \frac{V_c}{R_c C_c} e^{\frac{t}{R_c C_c}} = \frac{1}{C_c} e^{\frac{t}{R_c C_c}} \left(C_c \frac{dV_c}{dt} + \frac{V_c}{R_c} \right) \tag{3.13}$$

This derivation can be applied in equation 3.12 so that it becomes a separable differential equation,

$$\frac{I_p}{C_c} e^{\frac{t}{R_c C_c}} = \frac{d(V_c e^{\frac{t}{R_c C_c}})}{dt} \tag{3.14}$$

which can be solved for the voltage across the surface layer, integrating the left hand side of the equation.

$$V_c(t) = \frac{1}{C_c} e^{\frac{-t}{R_c C_c}} \int_{t_0}^{t} I_p(\tau) e^{\frac{\tau}{R_c C_c}} d\tau + V_c(t_0) e^{\frac{t_0 - t}{R_c C_c}} \tag{3.15}$$

The voltage can be approximated applying the trapezoid rule to the integral in the right hand side of the expression.

$$V_c(t) = V_c(t_0) e^{-\frac{t-t_0}{R_c C_c}} + \frac{t - t_0}{2C_c} \left(I_p(t) + I_p(t_0) e^{-\frac{t-t_0}{R_c C_c}} \right) \tag{3.16}$$

This expression as it is written allows to introduce a new variable: $\Delta t = t - t_0$, which can be defined as the time between two measurements. Besides, one should not forget that the experimental data contains a finite number of points of the current function, in other words, it is a discrete function. With these considerations, equation 3.16 can be rewritten as:

$$V_c^n = V_c^{n-1} e^{-\frac{\Delta t}{R_c C_c}} + \frac{\Delta t}{2C_c} \left(I_p^n + e^{-\frac{\Delta t}{R_c C_c}} I_p^{n-1} \right) \tag{3.17}$$

This expression allows to determine the voltage across a contamination layer of capacitance C_c and resistance R_c from the values of the probe current only. A final consideration regarding

3.17 is that it needs an initial condition, which can be interpreted as the charge of the capacitor at the beginning of the sweep and since there is no charge in the circuit before the sweep starts it is neglected.

$$V_c^0 = 0 \tag{3.18}$$

3.4. Characterization of the contamination layer

Although the method previously described is expected to provide very accurate results for the voltage in the surface layer, it is not that useful in the way it is formulated. Expression 3.17 requires as input data the values of the capacitance and resistance of the contamination layer which are obviously unknown.

However, let´s assume a pair of values for the resistance and capacitance of the surface contamination layer and through equation 3.17 calculate the voltage across the contamination layer. Then, it is possible to determine the voltage in the surface of the probe with expression 3.1:

$$V_p = V_b + V_s - V_c \tag{3.19}$$

The potential in the surface of the probe is the one that drives the plasma flow and, according to the theory of current collectors, the current drawn by the probe is unique for each potential. This means that when the current through the probe is plotted against the voltage in the surface of the probe, the result should be a single curve which should not show a hysteresis loop.

This feature is of great interest since when plotting the experimental data, bias voltage against probe current, a hysteresis loop shows up. But, if the voltage across the contamination layer is subtracted from the bias voltage, both branches of the loop should fall on top of each other. (Note that in equation 3.19 the spacecraft voltage is a constant that does not affect the loop and only shifts horizontally the I-V curve). Obviously, this will only be the case if the values of the resistance and capacitance of the contamination layer are appropriate.

Thus, one could iteratively search the electrical properties of the surface layer, resistance and capacitance, until the hysteresis is removed from the current characteristic. As a result of this process, one should be able to estimate the values of the capacitance and resistance that better suits the experimental data.

This problem can be solved with an optimization method, where the state variables are the resistance and capacitance and the objective function is the area of the hysteresis loop. This area can be easily calculated from the data. One needs to identify the two sections of the sweep, the forward and the backward parts, or, alternatively, locate the maximum voltage. Once they are identified and separated, the area is given by the expression:

$$Area = \left| \int_{V_{min}}^{V_{max}} I_{p_{forward}}(V)dV - \int_{V_{max}}^{V_{min}} I_{p_{backward}}(V))dV \right| \tag{3.20}$$

Thus, the goal is to get the area as close as possible to zero, to minimize its value. There are several algorithms available to do it, generally grouped into genetic algorithms and gradient-based algorithms. A genetic algorithm was chosen since it offered some advantages and the computational cost was affordable since there are only two variables (resistance and capacitance). No further discussions about the selection of the algorithm will be done here. The interested reader can find a more detailed exposition on optimization algorithms in [14].

The selection of a genetic algorithm has the advantage that no initial point is required and thus the solution does not depend on this initial guess. However it is required an estimate of the value of the parameters to set reasonable boundaries to the search domain. These estimates come from reference [5].

3.5. I-V characteristic fitting process

If successful, the process described allows to obtain an unique I-V curve that corresponds to the current characteristic described in the theory of current collectors. Is should be possible, then, to derive the plasma properties and the spacecraft potential from this curve applying an adequate fitting scheme. There is an standard and well-known fitting process that has been used in several missions such as Rosetta [15] or Maven [6]. However, it will be developed and described in depth in this report, including some alternatives and discussing their advantages and disadvantages against the standard procedure.

The I-V curve is divided into three regions as previously explained: ion saturation, electron retardation and electron saturation. Each of these regions, adequately processed, provides specific information. For example and in the simplest case, the ion saturation region can be used to determine the value of the ion density.

The first step in the fitting process is to separate the total current measured in the probe into the two contributions: the ion current and the electron current. In order to achieve this, one needs to identify the ion current which drives the curve in the ion saturation region. A simple way to isolate the ion current is to calculate the floating potential which is the potential where the ion current and the electron current cancel each other, which means that the total current is set to zero:

$$I_p(V_F) = 0 \tag{3.21}$$

Once the floating potential is known, it is clear that the ion current will dominate the range from -5V to V_F. However, in the upper end of the region, near to V_F, the electron current becomes as important as the ion current, but since it decays as an exponential, the effects are very localized. Besides, in the first measures near -5V sometimes show irregularities that can disturb the fitting. Thus, it seems reasonable to decrease the range by removing the tails. The decision taken was to remove a 5 percent of the length of the region in each end. Then, the ion current will be defined in the following domain;

$$5 + 0{,}05 \cdot (V_F + 5) < V_b < V_F - 0{,}05 \cdot (V_F + 5) \qquad [V] \tag{3.22}$$

In the region thus defined, the current curve should be linear and answer to the following expression:

$$I_i(V_b - V_c) = -I_{i0}(1 - \frac{V_b + V_s - V_c}{E}) \tag{3.23}$$

This expression can be properly rearranged in the form of a polynomial equation of first order,

$$I_p(V_b - V_c) = p_0 + p_1(V_b - V_c) \tag{3.24}$$

where p_1, which is the slope of the function, is defined as:

$$p_1 = \frac{I_{i0}}{E} \tag{3.25}$$

And finally, introducing the expression of I_{i0} and solving for the plasma density,

$$n = \frac{p_1 E}{\pi a^2 e v_d} \tag{3.26}$$

The error in the determination of the density is directly proportional to the error of the slope when interpolating the current curve. To minimize it, a procedure focused on getting rid of the outliers is followed: in the first iteration a linear interpolation is done to the experimental data and an initial value of the slope is obtained, then, the error, or deviation, of each point individually is computed and saved. The point with the largest error is removed from the data set and a new interpolation is performed and a new value for the slope is calculated. This new value is compared to the initial one and if it shows a variation of more than a 3 % of its value, then the point is discarded. This process continues until the algorithm finds a point where the value of the slope converges.

Figure 3.3 shows the procedure to obtain the plasma density. The first step is shown in graph *a*), where the ion current was isolated by calculating the floating potential, close to $3V$. Then graph *b*) displays the final interpolation of the curve where both the tail and the outliers were removed from the data. In graph *c*), the residuals are plotted and it confirms that the largest source of error are still the outermost points of the curve.

The first outcome of this analysis is the plasma density estimate, but also, more importantly, it allows to determine the ion current and subtract it from the measured current so that what is left is the electron current.

When subtracting the ion current one should be careful and consider the upper limit of the ion current which is defined in the ion ram energy, E, with the expression,

$$V_s + V_b - V_c < E \tag{3.27}$$

The maximum value of the bias voltage is $5V$ which is slightly higher of that of the ion ram energy, $4{,}9V$. However, the spacecraft potential is assumed to be negative and large enough

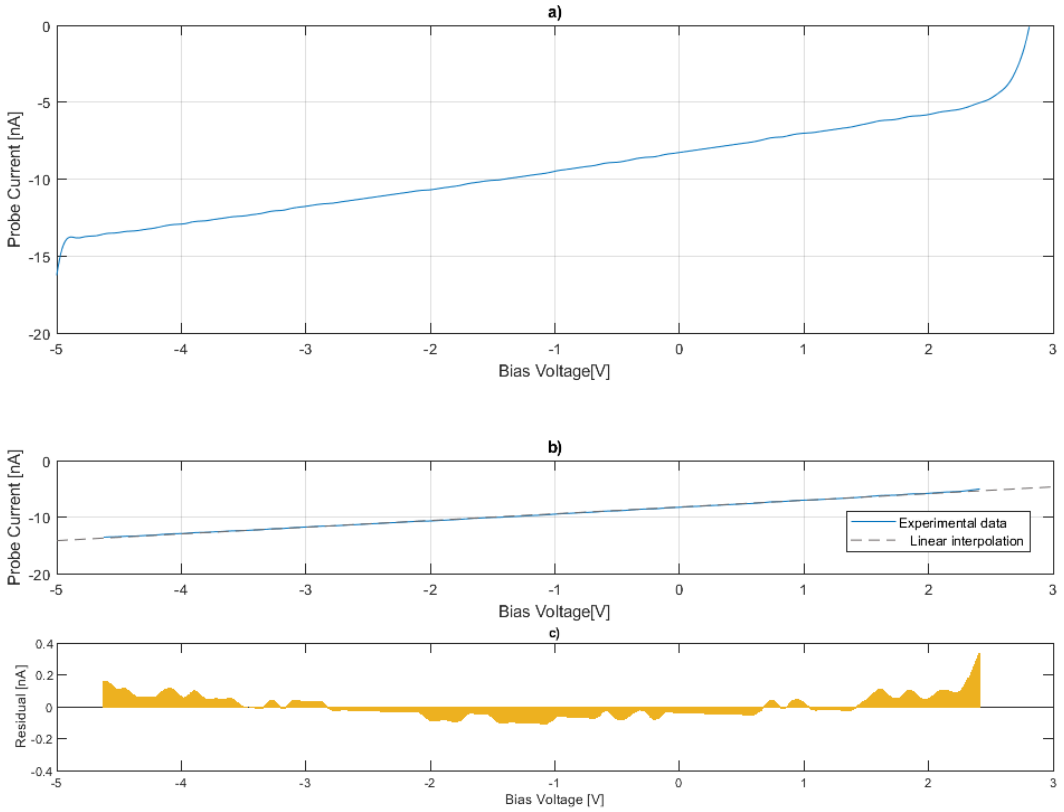

Figure 3.3: (a) Region of the current characteristic starting at the beginning of the sweep up to the floating potential. (b) Isolated ion curve and linear interpolation. (c) Residuals of interpolation of the experimental data with a polynomial expression. Data from satellite C on 05-Nov-2018 at t = 0h32′42″.

to compensate the $0{,}1V$ difference. Thus, it is reasonable to subtract the current in the whole sweep. The validity of this assumption will easily be checked with the results of the fitting process.

Eventually, the result of this process is the electron current. It is divided, as previously described, into two different regions: electron retardation region and electron saturation region. In particular, the electron retardation region is of special interest since it alone is able to provide the electron temperature. Two methods are going to be discussed. One is the standard one based on the logarithmic properties of the function and the second one, which is introduced in this report, is, to out knowledge, a new method based on the integral of the function.

The electron current in the retardation region is given by the expression:

$$I_{e_{ret}} = I_{e0} e^{V_p/Te} \tag{3.28}$$

And taking the logarithm of this equation it is possible to obtain a linear expression of the current,

$$ln(I_{e_{ret}}) = ln(I_{e0}) + V_p/T_e \tag{3.29}$$

which allows for a linear fitting as well as in the ion current. The electron temperature is then given by,

$$T_e = \frac{1}{p_1} \tag{3.30}$$

where p_1 is the slope of the linear interpolation.

Equation 3.29 is applied to an experimental measurement and plotted in figure 3.4, where the retardation region is highlighted between the dashed vertical lines. The function, despite being experimental, shows a strong linearity. It is important to observe that the curve for the smallest values of the current becomes random. This is due to the fact that the measurement error becomes more significant for smaller values of the current. This requires caution when interpolating the curve and getting rid of those values.

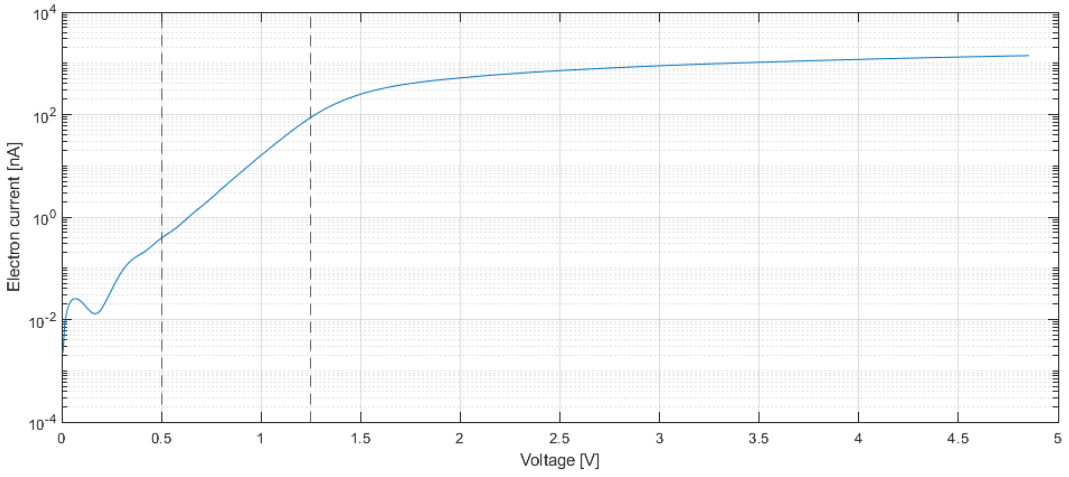

Figure 3.4: Electron current as function of the voltage in an experimental measure randomly selected. Y-axis in logarithmic scale to show the linearity of the retardation region (between the two dashed lines). Data from satellite C on 05-Nov-2018 at t = 0h32′42″.

Our alternative method to derive the electron temperature is through the integration of expression 3.28. The integral of the current yields the area under the curve which can be numerically calculated from the experimental data. The value of this area is directly proportional to the electron temperature and its expression is given by:

$$Area = \int_{V_0}^{V_1} I_{e0} e^{\frac{V}{T_e}} dV = I_{e0} T_e \left(e^{\frac{V_1}{T_e}} - e^{\frac{V_0}{T_e}} \right) = T_e (I_e(V_1) - I_e(V_0)) \tag{3.31}$$

This expression is very useful since it allows to determine the electron temperature using just any two points in the retardation region: the area between them divided by their current difference will provide the temperature.

This method avoids the irregularities found for the lower values of the current because one can select a high enough lower bound of the integral. However, reducing the size of the integration range generates more uncertainty in the result since small disturbances in the value

of the current cause significant errors in the estimation of the temperature. Thus, one must ensure that this interval is always sufficiently large to get reliable estimates.

Both methods show some constraints in its use but, nonetheless, they are pretty simple and reliable. Thus, the main challenge that one faces to obtain this estimate is to properly delimit the electron retardation region.

One can try to isolate this region by considering the derivative of the electron current given by equation 2.5. Differentiation has been used previously in other fields to obtain the plasma potential, such as in the inflection point method for cylindrical probes [16]. This method is the standard tool also for spherical probes [17] where the derivative of the electron current is given by:

$$\frac{dI_e}{dV_p} = \begin{cases} \frac{I_{e0}}{T_e} e^{\frac{V_p}{T_e}} & if \quad (V_p < 0) \\ \frac{I_{e0}}{T_e} & if \quad (V_p > 0) \end{cases} \tag{3.32}$$

According to this expression, the derivative of the function increases monotonously until it reaches a maximum value at the plasma voltage, which is then kept constant through the saturation region. Thus, with the derivative of the experimental data, calculated through finite differences (see Appendix A), it is possible to identify the upper limit of the retardation region.

Figure 3.5 displays the derivative of an experimental measure using the finite differences scheme.

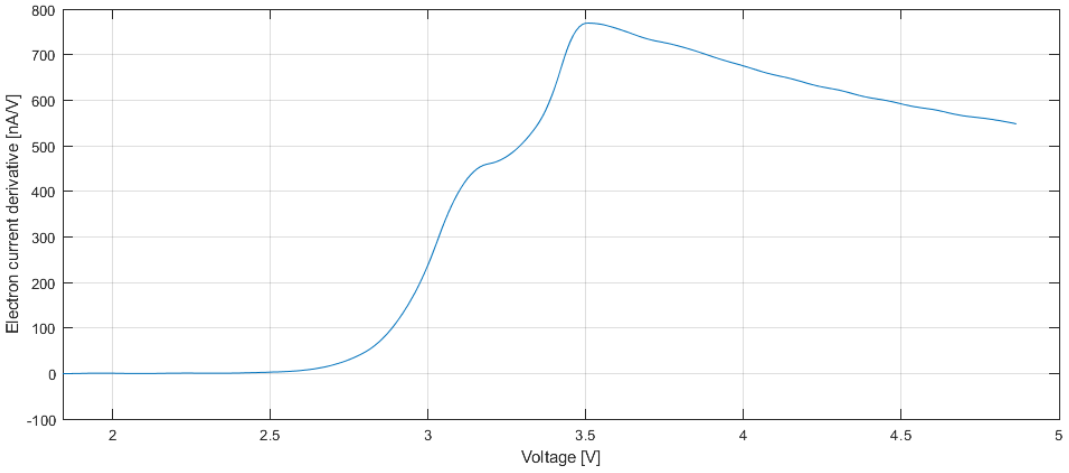

Figure 3.5: Electron current derivative of an experimental measure showing the electron retardation region and the electron saturation region. Data from satellite C on 05-Nov-2018 at t = 0h32′42″.

Figure 3.5 is of great interest since it shows two relevant features that are not explained with the model that is being tested.

The electron saturation region has been said to have a constant derivative according to the theory of current collectors for a spherical probe. However, the graph in figure 3.5 clearly shows a monotonically decreasing function in the uppermost region of the sweep.

The current response in the electron saturation region depends on the geometry of the probe. For cylindrical probes, the current is proportional to the square root of the probe voltage [18], according to equation 3.33.

$$I_e = I_{e0}\frac{2}{\sqrt{\pi}}\left(1+\frac{V_p}{T_e}\right)^{1/2} \tag{3.33}$$

Under ideal conditions the saturation current to a spherical probe should be proportional to the voltage, as in equation 2.9. However, these conditions are impossible to meet exactly in the reality. For example, the spherical probe needs to be attached to the spacecraft by a rod. As a consequence, the probe is not an isolated sphere because part of the surface is occupied by the rod, which, in the end, distorts the elctric field from the probe. As a result, the behaviour is not ideal, but fairly close to it.

The real current response in the saturation region is then better described neither by the cylindrical response nor the spherical, but by an intermediate behaviour [6] such as in:

$$I_e = I_{e0}\left(1+\frac{V_p}{T_e}\right)^{\beta} \tag{3.34}$$

where β is a coefficient that can take a value between 0.5 (cylinder) and 1 (sphere). In the case of a spherical probe, the higher the disturbance, the lower the value of β.

With this modification to the theory, it is possible to obtain the value of the derivative in the saturation region in order to validate it with the data measured with Swarm probes.

$$\frac{dI_e}{dV_p} = \beta\frac{\frac{I_{e0}}{T_e}}{\left(1+\frac{V_p}{T_e}\right)^{1-\beta}} \tag{3.35}$$

Equation 3.35 is, in fact, a monotonically decreasing function which fits with the experimental derivative behaviour. However, the value of the derivative for a probe voltage equal to the plasma voltage differs from that of the retardation region ($\frac{I_{e0}}{T_e}$, see equation 3.32):

$$\frac{dI_e}{dV_p}(V_p=0) = \beta\frac{I_{e0}}{T_e} \tag{3.36}$$

This means that the current characteristic should show a discontinuity in its slope, i.e. in its derivative function. This jump in the derivative is of $(1-\beta)$ relative to the value of the derivative in the electron retardation region.

One should not expect a sudden change in the current characteristic such as this jump, and it is indeed not observed in the experimental data, figure 3.5. Conversely, it appears that the derivative is smoothed already from the electron retardation region.

Precisely this transition between the electron retardation region and the electron saturation region shows some strange features that strongly differ from that expected with the

theory. It appears that the real circumstances have effects on the measurements that are not well explained with the current theory.

The first implication of the effects of these non-ideal conditions is that the electron saturation region is not useful to derive the plasma properties, since the parameter β is unknown. The only way to calculate it is to fit the saturation region to equation 3.34, for which the temperature and the density are required.

Besides, the region around the plasma potential shows values that are unreliable to derive any parameters. As a consequence, the spacecraft potential cannot be accurately defined, but it is only possible to give a range of values where it is expected to be found.

Nevertheless, the differentiation allows to divide the electron current into two regions, one that contains the electron retardation current and the other one that contains the electron saturation current. Thus, it allows to define a region to interpolate the experimental data, where the upper limit would be defined by the peak in the derivative.

The lower limit is set to get rid of the measurement errors when the current is too small. This can be solved by setting a fraction of the maximum current found in the region as the lower limit, for example, a 5 %. This maximum current corresponds to potential where the peak in the derivative is located, V_{peak}:

$$I_{e_{max}} = I_e(V_{peak}) \tag{3.37}$$

The result of this procedure is shown in figure 3.6. Graph a) in the figure shows the initial electron current curve and graph b) shows the curve after finding the peak in the derivative and removing both ends of the curve. What is left is a region where the linear behaviour of the electron retardation region should be found.

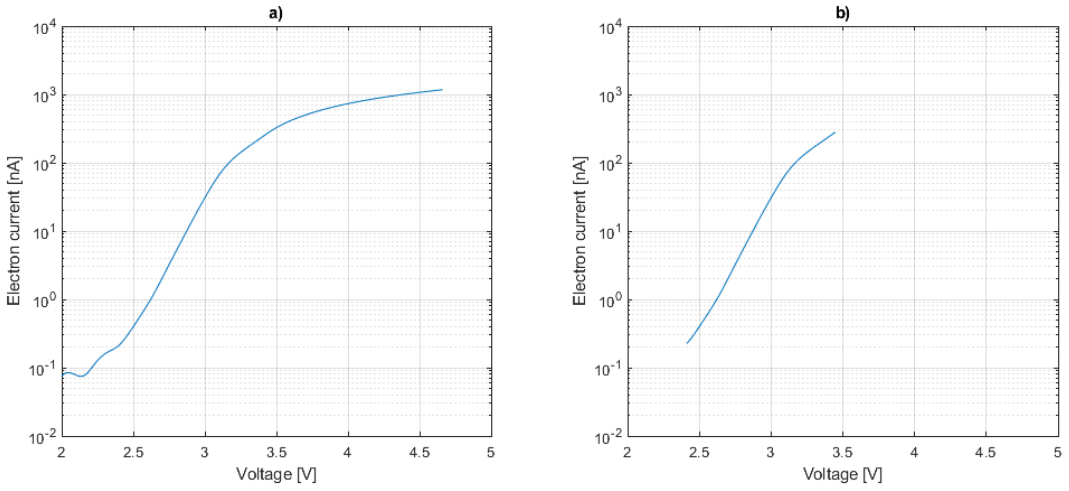

Figure 3.6: Electron current of an experimental measure showing a) the complete range of the current, b) the electron retardation region isolated from the saturation region and removing the initial values. Data from satellite C on 05-Nov-2018 at t = 0h32′42″.

Graph b) in figure 3.6 allows to derive the electron temperature applying any of the two methods described: either by linear interpolation or by integration. But instead of working with

the whole graph, the methods will be applied only to sections of it, in a procedure described below.

The electron current in the electron retardation region is stored in an array of length N. Then, a section is defined as a group of $0{,}1N$ data points. This means that the section length is 10 percent of the total length. In case the section length is shorter than 0.1V, this value is used instead, which means that any section will never be shorter than 0.1V.

The first section will start at the first value of the whole array and both will share the first $0{,}1N$ points. Then, the electron temperature will be derived for this particular section in order to be stored. Then the same will be done for the second section that will start in the second value of the array and share the next $0{,}1N - 1$ points.

In general, the section number k, will start in the k position in the array and last until the $k + 0{,}1N - 1$. The last section will start at the position $k = N + 1 - 0{,}1N$, which also means the total number of sections evaluated. Taking for example an electron retardation region that starts at 1V at ends at 2.5V and has 114 data points the section length is of 12 points and the number of sections and, therefore, temperature estimates is of 103.

These temperature estimates are plotted in a histogram of $0{,}005eV$ band width. This allows to group the different estimates of each individual section to identify the wrong estimates due to a) the noise in the lower part of the region and b) the non-ideal effects near the plasma voltage. The bin with the higher number of sections, and thus with the higher number of similar temperature estimates, will be used to define the electron temperature. The electron temperature will be defined then as the mean value of all the temperature estimates contained in the bin with the higher number of sections.

An example of this histogram is shown in figure 3.7. The histogram shows temperature estimates ranging from $0{,}155eV$ to $0{,}265eV$. However, many of them are unique, revealing they come from non-regular areas.

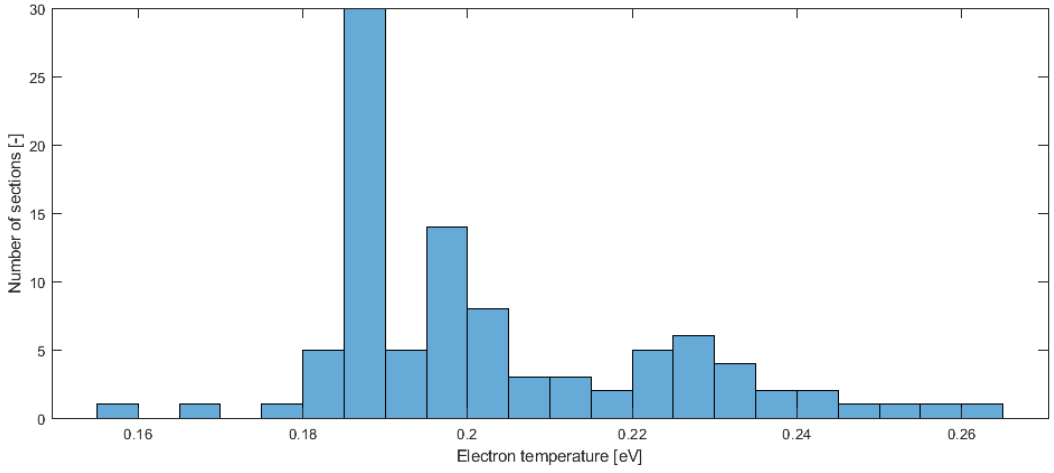

Figure 3.7: Histogram of electron temperature estimates grouped in bins of 0.005V band width. Data from satellite C on 05-Nov-2018 at t = 0h32′42″.

The histogram shows that the maximum number of estimates, 30, is located in the bin of $[0{,}185, 0{,}19]eV$. The mean value of all the 30 estimates is, in this particular case, of $0{,}1869eV$.

Finally, this is the method that is going to be used to characterize the surface contamination layer through the parameters of the resistance and the capacitance and to derive the values of the plasma density and electron temperature. This scheme is going to be applied to several measurements of the Langmuir probes of the three Swarm satellites so that a statistical analysis on the data can be performed and the results compared with previous estimates.

4. Results

In this section, the procedure describe in the previous chapter has been applied in order to present its results. These results are going to be analysed and discussed to derive adequate conclusions regarding the model and/or the method used.

4.1. Simulated I-V characteristics

Equation 3.9 is numerically integrated with the parameters listed in table 3.1. The simulation is done for different values of resistance and capacitance, taking the values given in [5] as reference.The results are shown and discussed in the following figures.

Figure 4.1 shows how the I-V characteristic changes when the resistance of the surface layer is modified, comparing it with the *'clean probe'* case. The graph shows how the smaller resistances (10 and 100 $k\Omega$) have little to no effect in the measured current. If one takes the maximum value of current recorded in this specific measure and multiply it for the resistance of $100k\Omega$ the voltage drop is of about $0{,}07V$, which is almost unnoticeable.

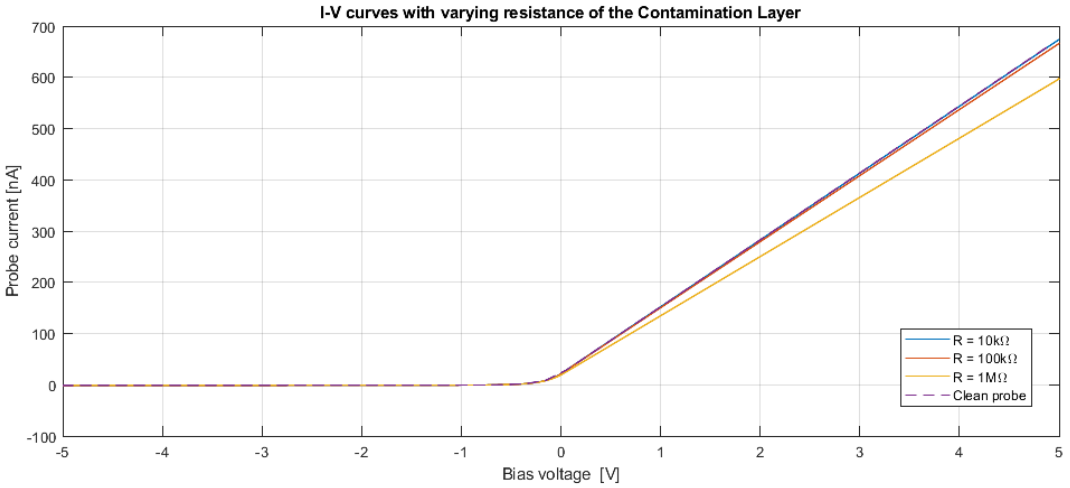

Figure 4.1: Simulated current characteristics with varying resistance values keeping the capacitance constant at a value of $1\mu F$

Besides, the graph shows no hysteresis loop in neither of the three cases. This implies that the capacitor was not charged and the plasma current went primarily through the resistor as a 'leakage current'.

Figure 4.2 shows how the I-V characteristic changes when the capacitance of the surface layer is modified, comparing it with the *'clean probe'* case. The graph shows that it is not possible to reproduce the hysteresis loop with a resistance of $100k\Omega$ with the data measured

with Swarm. The solution adopted was to increase the resistance value, i.e. to decrease the leakage current, so that the current is forced to go through the capacitor.

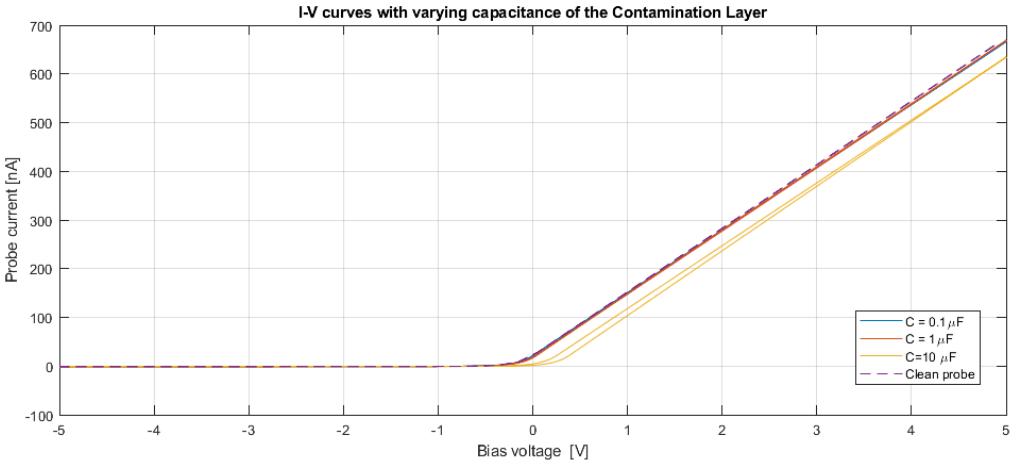

Figure 4.2: Simulated current characteristics with varying capacitance values keeping the resistance constant at a value of $100k\Omega$

Figure 4.3 is similar to figure 4.2 but the resistance has been increased to $1M\Omega$. In this case the hysteresis loop is noticeable in two of the cases: $1\mu F$ and $0{,}1\mu F$. The greater loop, though, is got with the lower capacitance.

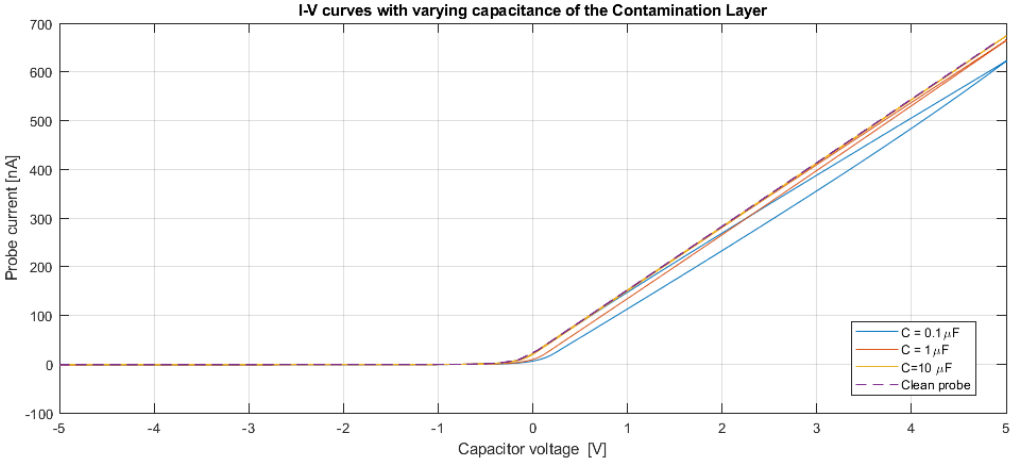

Figure 4.3: Simulated current characteristics with varying capacitance values keeping the resistance constant at a value of $1M\Omega$

This last figure proves that the model is able to reproduce the hysteresis loop found in the experimental measures of the Langmuir probes on Swarm (see figure 2.6). The main takeaway from this initial review of the model is that the resistance of the surface layer might be significantly higher than the values found in the literature.

4.2. Computation of the contamination layer: values of capacitance and resistance

The results of the optimization to characterize the contamination layer were really insightful. The results prove that the RC model is not only able to qualitative explain the hysteresis loop, but to quantitatively characterize it in a simple formulation. The results have shown that it is possible to find a certain pair of values that completely remove the hysteresis loop of the experimental data. This is shown for example in figure 4.4 where the hysteresis loop observed in graph a) is completely removed after applying the model and subtracting the potential of the surface layer.

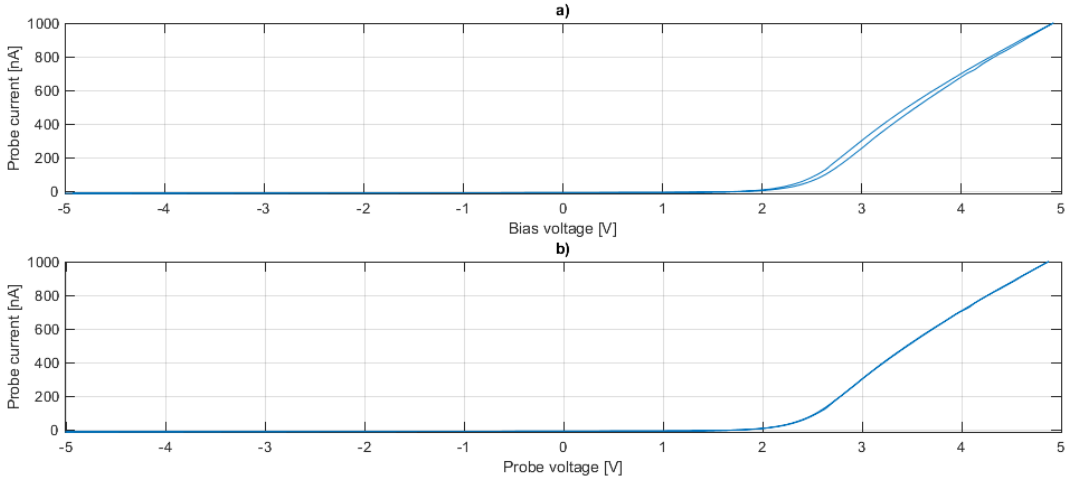

Figure 4.4: Change in the current characteristics using the RC model to remove the hysteresis cycle. a) Raw data from the measurements. b) Current characteristic of the probe without the hysteresis loop. Data from satellite B on 20-Nov-2018 at t = 3h10′22″.

Another meaningful result is that the value of the surface layer resistance was not relevant in this computation. The optimization always tried to make the resistance values as high as it could no matter how high the upper limit it was and if I forced solutions with a lower resistance the method was not able to provide an accurate result. As discussed before in figures 4.1, 4.2 and 4.3, the behaviour of the current characteristics clearly shows that the leakage resistance is significantly higher than other studies have found it their instruments. For practical purposes, it can be assumed that there is no leakage resistance in the Swarm Langmuir Probes.

However, the surface contamination does introduce a capacitive behaviour in the measurements that is accurately defined by the capacitance. Figure 4.5 shows the values of the capacitance arranged by satellite and probe in six different histograms. This figure, and the following, are based on the measurements contained in the files:

- $SW\_EXTD\_EFIA\_LPSIV\_20181029T000023\_20181029T235815\_0102.cfd$ for satellite A.
- $SW\_EXTD\_EFIB\_LPSIV\_20181120T000030\_20181120T235822\_0102.cdf$ for satellite B.
- $SW\_EXTD\_EFIC\_LPSIV\_20181105T000042\_20181105T235834\_0102.cdf$ for satellite C.

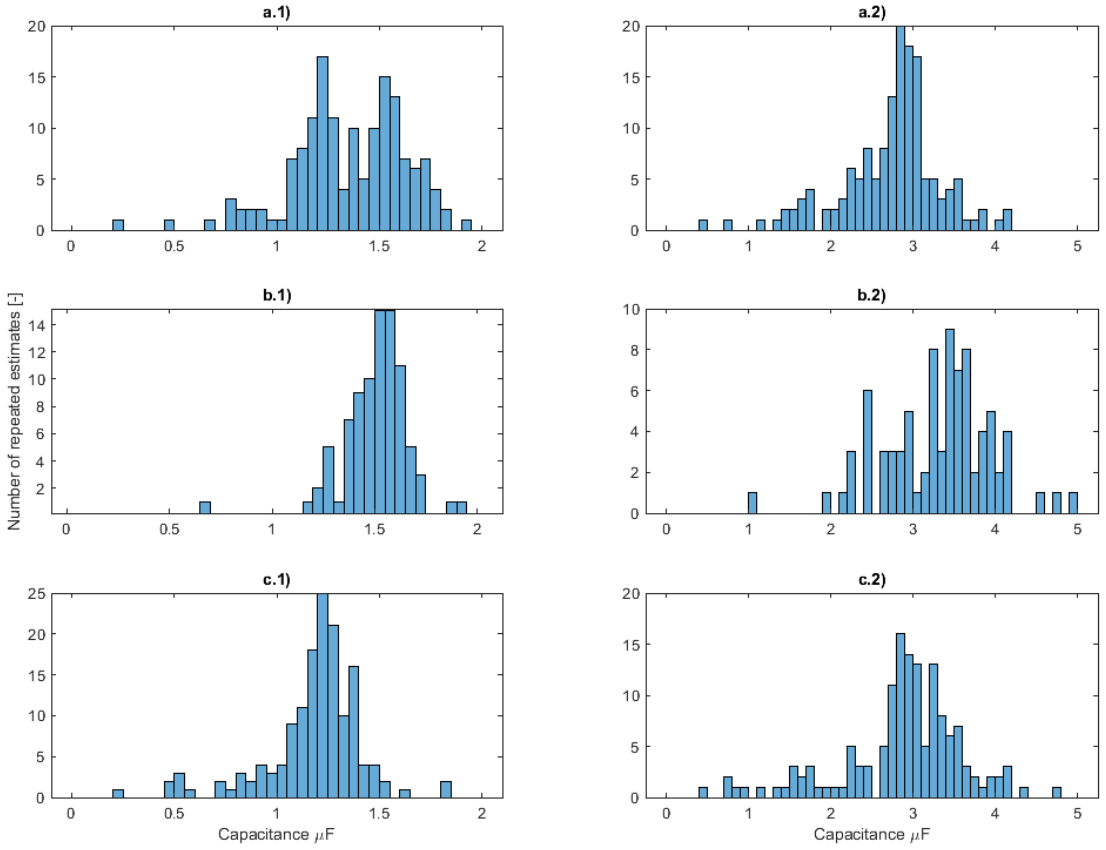

Figure 4.5: Histogram of capacity values in the the three satellites: satellite A (a.x), satellite B (b.x) and satellite C (c.x); and also for both probes in each satellite: probe 1 (x.1) and probe 2 (x.2).

The first conclusion that can be derived when observing the histograms is that probes 1 on every satellite have a slightly lower capacitance, in the range of 1 to 2 μF, than the capacitance of probes 2, between 2 and 4 μF. This fact suggests that the Au electroplating applied to probes 2 managed to increase the capacitance by decreasing the width of the contamination layer.

Besides, it seems that the peaks in both $b.x$) histograms are slightly shifted to the right. This could suggest that since satellite B is in a higher orbit and the concentration of pollutants is reduced the contamination layer developed in satellite B is thinner than that in satellites A and C in a lower orbit.

4.3. Plasma parameter estimates

The RC model proved successful to remove the hysteresis loop from the experimental data for a number of test cases and thus allowing to calculate unique I-V characteristics that are explained to a large degree with the usual equations of current collectors in plasmas. The method then described allowed to systematically derive the values of the plasma density and

the electron temperature from the appropriate current characteristics.

The first parameter, the plasma density, is derived from the ion current in the ion saturation region. The linear fitting of the current curve allows to derive the plasma density as previously described. The values of the density obtained with this procedure are given in figure 4.6, arranged also by satellite and probe in six histograms.

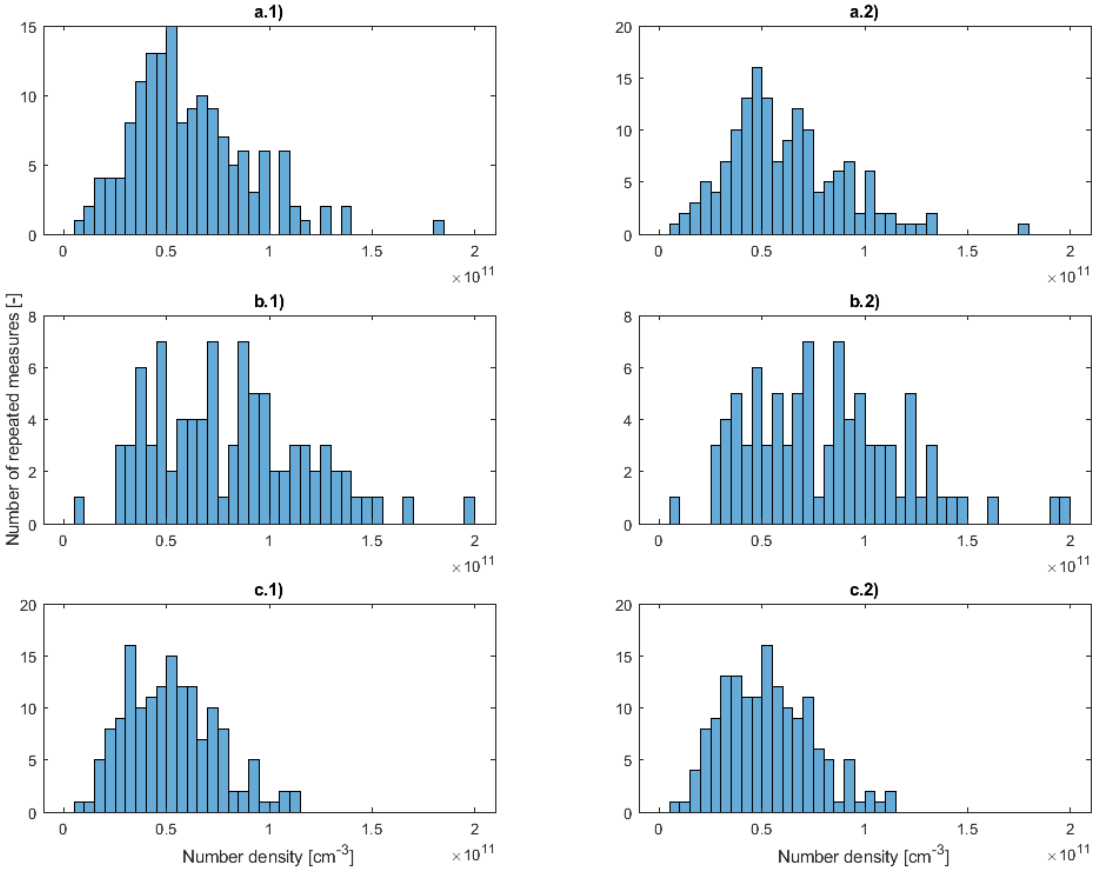

Figure 4.6: Histogram of density values in the the three satellites: satellite A (a.x), satellite B (b.x) and satellite C (c.x); and also for both probes in each satellite: probe 1 (x.1) and probe 2 (x.2).

Unlike with the capacitance histograms, this figure does not show a difference between the two probes on each satellite. This agreement between both measures was expected since they are operated in the same environment and in the same time and the low currents involved in the I-V region, where they were derived from, prevented the capacitor to charge and modify the probe measure.

Again, satellites A and C, that travel in close orbits, show similar values for the plasma density, centered around $5 \cdot 10^{10} m^{-3}$. However, satellite B estimates are incongrous. The values of density are more disperse, with no clear average value and also somewhat higher than those of satellites A and C. This behaviour can have different causes. The measurements of the three satellites come from different days and the ionosphere suffer changes that could lead to

a increase in the plasma density. Or it could be a consequence of some bias in the manual selection of the measurements to process.

The second parameter, the electron temperature is derived from the electron current in the electron retardation region. Two methods were described to obtain the value of the electron temperature from the I-V curve. Here, the linear logarithmic fitting was used in order to calculate the temperature. The results are shown in figure 4.7 arranged by satellite and probe in six histograms.

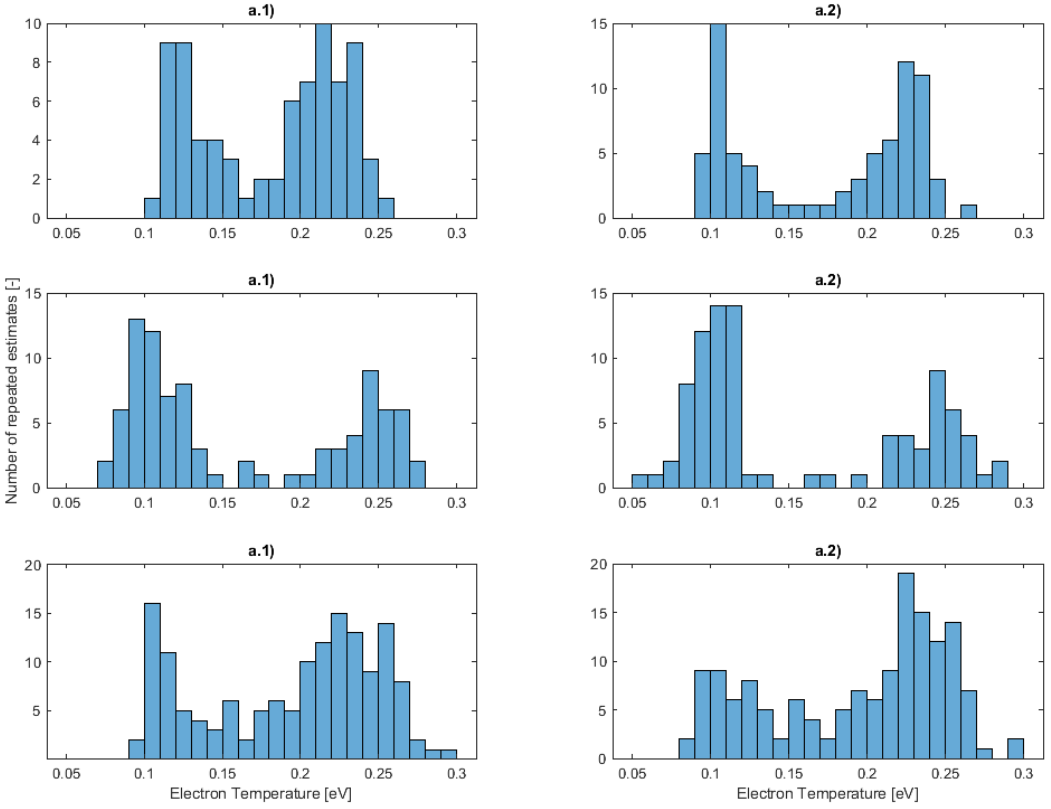

Figure 4.7: Histogram of temperature values in the the three satellites: satellite A (a.x), satellite B (b.x) and satellite C (c.x); and also for both probes in each satellite: probe 1 (x.1) and probe 2 (x.2).

All six histograms are significantly similar and consistent with each other. The main feature that can be found in the graphs is that all histograms show two peaks: the first one around $0{,}1eV$ and the second one around $0{,}23eV$. Both peaks are equally significant in number of measurements. This suggest that the satellite encounters two different plasma environments throughout its orbit. One of them is much hotter than the other, whose electron temperature is approximately half.

One can also notice that satellite B shows minor differences with the other two satellites. The cold region is rather colder with some measurements well below $0{,}1eV$ and the warm region has the peak shifted to $0{,}25eV$ instead.

Another important feature that is shown in figure 4.7 is that the temperature estimates of probes 1 and 2 do not fully match with each other. Figure 4.8 is a bar graph comparing the temperature estimates of each probe in every measurement for the case of satellite C.

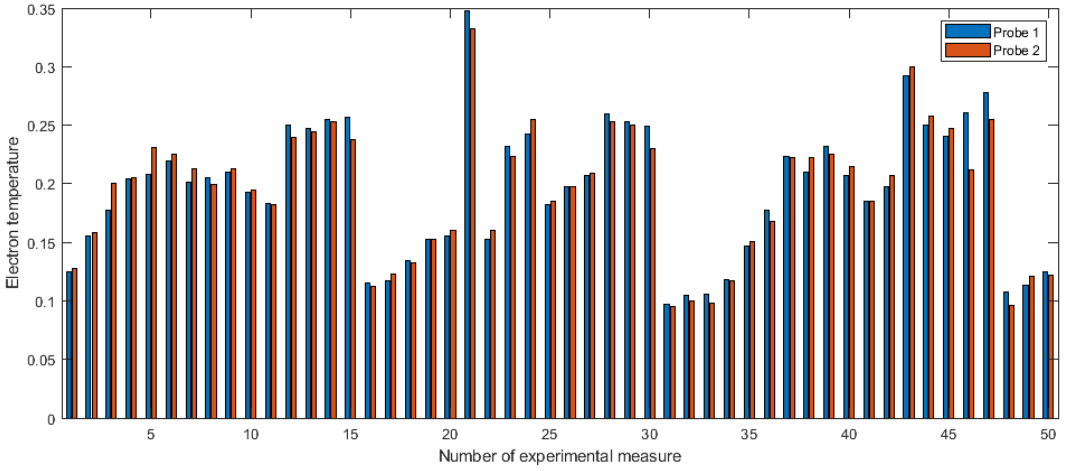

Figure 4.8: Values of the temperature estimates for both probes in satellite C compared. Blue color for probe 1 and red for probe 2.

Figure 4.8 shows that generally the result on probe 1 and probe 2 are fairly precise, see measurements 19,26 or 41. However, there are strong disagreements such as in 21, 46 or 47. Besides, there is no clear bias in the estimates, neither probe 1 provides higher temperatures nor does probe 2.

Another feature of figure 4.8 which makes it quite interesting is that it shows how the temperature increases with time up to a point at which it suddenly drops to a much lower temperature. This fact strenghens the belief that the satellite encounters two environments in its orbit.

4.4. Final comments

In the initial data analysis, it was argued that one of the irregular features that the Swarm Langmuir probes have shown is that the current-voltage measurements of the two probes that each satellite carries did not match each other. Thus far, nothing has been discussed about this and, in fact, the RC model itself cannot explain this behaviour.

The RC model is an useful tool to remove the hysteresis cycle as it shows figure 4.9. When comparing graph a) and b), the improvement in the measurement is noticeable. However the two probes give current characteristics that are quite different. Even after shifting in voltage, the curves are not fairly identical. This suggest the presence of another mechanism that is altering the measurements.

In [6] have found that the main obstacle when fitting the I-V curves was the contribution of a surface resistance on the sensor. This surface resistance had a major impact in the electron

retardation region leading to inaccurate temperature estimates. This scheme was tried in the Swarm measurements.

The only modification is to introduce another resistance in series with the capacitance. This scheme, however, failed since there is no possible way to unequivocally identify the value of the resistance in each probe, but only the difference between them. This is due to the linearity of the function tested, see [6].

Thus, one can obtain the voltage drift and the difference in resistance in the two probes by forcing the current characteristics to fall on top of each other. This is shown in graph c) of figure 4.9.

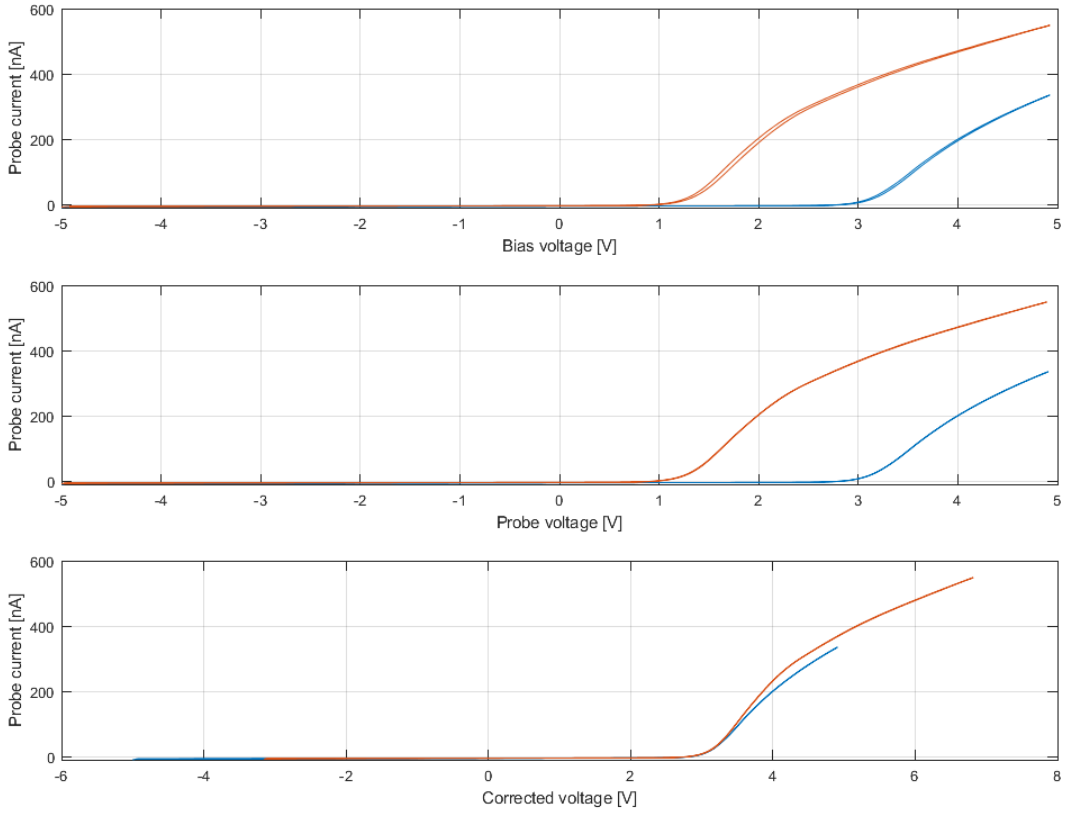

Figure 4.9: Current characteristics curves of a single measurement: a) Experimental raw data b) Current characteristic where the hysteresis loop has been removed with the RC model and c) Curve adjustment with a $\Delta R = 150k\Omega$ and a $\Delta V = 1{,}85V$. Data from satellite C on 05-May-2018 at t = 0h34′50″.

Figure 4.9 shows how the usage of another resistance in series, along with the voltage drift, is able to correct the disagreement between the two probes to a large degree. In the case shown the voltage drift was of $1{,}85V$ and the difference in resistance was of $150k\Omega$.

In every case tested, probe 2 always showed a lower resistance around $100 - 200k\Omega$. This is reasonable since the second probe received the surface tratment, Au electroplating, to reduce the surface contamination layer.

Nevertheless, this model and this feature requires a deeper research and understanding regarding the Swarm measurements since it could greatly affect the temperature estimates.

5. Conclusions and future work

The research question of this work was if the RC model proposed is a suitable tool to correct the data and improve the plasma parameter estimates from Swarm satellites. This has driven all the work done under this project and also is the essence of this report. To find an answer to this question several steps were needed: deriving the expressions of the model including the contamination layer, using the experimental data to calculate the values that define this external layer and then extending the analysis to several measures and assess the reliability of the model. In the end, the results confirmed the validity of the model but with some exceptions.

The surface layer was computed and the values of the resistance and capacitance calculated. However, the results were highly unexpected. The resistance of the contamination layer was quite high, or at least high enough to not affect the measurements. What this means is that there is no leakage current in the probes. A possible interpretation for this is that the insulating external layer is uniformly distributed throughout the whole surface of the spherical probe. Therefore, all the particles reaching the probe from the plasma end up charging the capacitor.

It was possible to determine the value of the capacitance of this layer. It was of approximately a few microfarads in the events studied. One of the probes in each satellite received a surface treatment to protect the probe from the environment and avoid oxidation. This resulted in a different behaviour that was observed with the results of this project. The probes with the surface treatment had a capacitance of $3\mu F$, while the other group of probes with no treatment showed a capacitance of $1{,}5\mu F$. In an ideal capacitor this would mean that insulating layer is twice as wide in the unprotected probes.

Nevertheless, the RC model as described was able to explain the hysteresis loop present in the experimental measurements. And it was successful in accurately calculating the potential across the contamination layer. Thus, it was possible to subtract it from the bias voltage and obtain the standard current characteristics. This definetely, was a remarkable improvement in the measurements that allowed for more precise and presumably more accurate estimates of the plasma parameters.

However, this model could not explain all the irregularities found in the Swarm LP measurements. Measurements in probes 1 and probes 2 do not accurately match each other. In the origin of this disagreement one can find a voltage shift that could be caused by the $E \wedge B$ effect. But given the small separation between the probes, it is unlikely that it is fully responsible for the mismatch. Other sources of voltage jumps are in the contact potentials for example.

Apart from the voltage shift, it has been proposed to include a second resistance, between the probe and the surface layer in order to bring the curves of the two probes closer. However, we argued that the sweeps do not contain information enough to determine the resistance of both probes, but only their difference, due to the linearity of the expressions involved.

Future work will likely be focused on this issue, how this resistance can affect the accuracy of the plasma parameter estimates and how to unequivocally define the resistance in each probe.

Other aspect that should be answered in the future is how to reduce the disturbances that affect the electron saturation region. Since it is not possible to have the ideal case of a perfect sphere in the plasma, to know how the rod affects the plasma sheath around the probe tip would be valuable.

One of the main takeaways of this project is that when the theoretical world of the equations and ideal conditions gets closer to the real world full of pertubations and complexity, everything seems to disagree and nothing works properly or as expected. Thus, deriving the value of the electron temperature is not as simple as fitting a set of points. One needs to consider multiple aspects regarding the instrument measurement error, the external conditions of the probe, interferences of other elements of the spacecraft, etc.

In conclusion, this project managed to use the RC model to describe the hysteresis found in the data and, successfully, calculated the parameters that define the external layer, allowing for a significant improvement in the data analysis of the Swarm measurements. Thus, this work represents a valuable step towards an improved analysis method for the Swarm Langmuir Probes in particular, and for the missions that are to come in the future.

References

[1] Edward P. Szuszczewicz and Julian C. Holmes. Surface contamination of active electrodes in plasmas: Distortion of conventional Langmuir probe measurements. *Journal of Applied Physics*, 46(12):5134–5139, 1975.

[2] Swarm probes weakening of Earth's magnetic field. *http : //www.esa.int/applications /observing_the_earth/swarm/swarm_probes_weakening_of_earth_s_magnetic_field.*

[3] H. M. Mott-Smith and Irving Langmuir. The Theory of Collectors in Gaseous Discharges. *Phys. Rev.*, 28:727–763, Oct 1926.

[4] L. Lomidze et al. Calibration and validation of Swarm plasma densities and electron temperatures using ground-based radars and satellite radio occultation measurements. *Radio Science*, (53):15–36, 2018. https://doi.org/10.1002/2017RS006415.

[5] A. Piel et al. Plasma diagnostics with Langmuir probes in the equatorial ionosphere: I. The influence of surface contamination. *J. Phys. D: Appl. Phys.*, 34(2643), 2001. https://doi.org/10.1002/2017RS006415.

[6] R. E. Ergun, L. A. Andersson, C. M. Fowler, and S. A. Thaller. Kinetic Modeling of Langmuir Probes in Space and Application to the MAVEN Langmuir Probe and Waves Instrument. *Journal of Geophysical Research: Space Physics*, 126(3):e2020JA028956, 2021. e2020JA028956 2020JA028956.

[7] About Earth Explorers. *https : //www.esa.int/applications/observing_the_earth/future_eo/earth_explorers/about_earth_explorers*2.

[8] D. J. Knudsen et al. Thermal ion imagers and Langmuir probes in the Swarm electric field instruments. *J. Geophys. Res. Space Physics*, (122):2655– 2673, 2017.

[9] Luis Conde. An introduction to Langmuir probe diagnostics of plasmas. *Departament of Applied Physics, Universidad Politécnica de Madrid*, May 2011.

[10] E. Engwall. Cold magnetospheric plasma flows: Properties and interaction with spacecraft. *Licentiate dissertation, Inst. f. astronomi o. rymdfysik, Uppsala universitet*, 2006.

[11] F. Johansson. Numerical simulation of Rosetta Langmuir Probe. *Dissertation*, 2013.

[12] A. Gramin. Analysis of Calibration and Surface Contamination on the Rosetta Langmuir Probe Instrument. *Dissertation*, 2017.

[13] C.-G Fälthammar. Space Physics. *Department of Plasma Physics, The Royal Institute of Technology*, June 1991.

[14] Rajesh Kumar. Arora. *Optimization: Algorithms and Applications.* CRC Press, 2015.

[15] A. Eriksson, R. Gill, J. Wahlund, M. André, A. Mälkki, B. Lybekk, A. Pedersen, J. Holtet, L. Blomberg, and N. Edberg. RPC-LAP: The Langmuir probe instrument of the Rosetta plasma consortium. 2007.

[16] J. R. Smith, N. Hershkowitz, and P. Coakley. Inflection-point method of interpreting emissive probe characteristics. *Review of Scientific Instruments*, 50(2):210–218, 1979.

[17] A. Johlander. Photoemission on the Rosetta spacecraft. *Dissertation*, 2012.

[18] Sigvald Marholm and Richard Marchand. Finite-length effects on cylindrical Langmuir probes. *Physical Review Research*, 2(2), 2020.